TÉCNICO LISBOA

Design of a Green Sunshade: An Entrepreneurial Approach

Danish Rehman

Thesis to obtain the Master of Science Degree in

Energy Engineering and Management

Supervisor(s): Professor José Manuel Dias Ferreira de Jesus and Professor Enrique Velo

Examination Committee

Chairperson:	Professor José Alberto Caiado Falcão de Campos
Supervisor:	Professor José Manuel Dias Ferreira de Jesus
Member of the Committee:	Professor Luis Rego da Cunha de Eça

October 2014

Acknowledgments

I would like to thank all my teachers and colleagues who trusted in me and provided me the opportunity to have an exciting time during this period. I would specifically like to thank Mr. Dimitrios Panagiotakopoulos for being a wonderful and inspirational team member. I would also like to thank RENE program coordinator, Dr. Enrique Velo for accepting our idea of working in KIC incubator. A humble gratitude to my supervisors Drs. Toste Azevado (L) and Jesus de Feirreira for their support throughout this work. Availability of research libraries and softwares from KTH Bibliotek are also acknowledged, without which I would not have been able to perform this study. I would like to extend my gratitude to Mr. Francesco Ierullo from ASCAMM Barcelona who helped me through composite design.

I would like to pay deep gratitude to my parents for their unconditional love, support and prayers during these two years of master. And I pray to Allah who has bestowed me with this opportunity to use gained knowledge for the best of humanity.

Abstract

Numerical methods are employed in engineering applications to reduce the potential failures and even reduce the production times in industry. With the help of such numerical analysis qualitative as well as quantitative features necessary for a design that will meet the end user requirements can be estimated. The objective of present thesis is to design a wind resistant solar sunshade as a part of product development cycle. The importance of simulating the neutral atmospheric boundary layer in CFD for accurate estimation of wind forces over low rise structures has been explained. For validation of boundary conditions we perform flow analysis past a low rise TTU building and compare our results to that of field, experimental and other numerical studies. It is shown that the chosen set of boundary conditions results in a reasonably good approximation of pressure field around the building. Using the same set of boundary conditions we simulate flow past the sunshade at a $Re = 3 \times 10^6$ with 14.5% turbulence at the height of sunshade. We show that steady state RANS solution is comparable to unsteady which essentially means that flow is steady in statistical sense and there are no time dependent vortices shed as encountered in bluff bodies. 9 different wind incidence angles are simulated from 0^o to 240^o with 30^o interval to find out the extreme loading scenario. Results show that extreme loading is experienced at angles of 30^o and 0^o whereas all other loading profiles are encompassed in these two. Therefore we perform full scale CFD analysis at 0^o and 30^o so that generated pressure field can readily be used for defining structural loads. The area weighted average of pressure at 5 sub-regions of the sunshade is calculated and is used for verifying structural integrity. We then perform a FE analysis on two design schemes using reinforced plain weave glass fabric composite and industrial aluminum. Results have shown that composite is not suitable for the current application. Without any internal structure that is stiffeners, composite design with combined thickness of $5.4mm$ undergoes a deflection of $26.10mm$ at the leeward end of sunshade. On the other hand the design with aluminum pipes with a cross section of $20mm \times 20mm \times 2mm$ results in deflection of only $2.4mm$ which is in practical range with von-Mises stress of 10.4MPa giving a design with safety factor of 1.92. Furthermore the resulting weight from aluminum design is 9.07kg compared to 55.78kg in case of composite. Therefore a metallic design promises a lightweight and cheap solution for the sunshade under study and will be followed for manufacturing.

Keywords- Neutral ABL, Wind loading, Static structural analysis, Low-rise structure

Resumo

Hoje em dia, métodos numéricos são utilizados em aplicações de engenharia para reduzir as potenciais falhas e os tempos de produção na indústria. Com a ajuda destas análises numéricas, as características qualitativas e quantitativas, necessárias para um projeto que irá satisfazer as necessidades dos utilizadores finais podem ser estimados. O objetivo do presente trabalho é a concepção de um guarda-sol resistente ao vento como parte do ciclo de desenvolvimento do produto. A importância da simulação da camada limite atmosférica neutra em CFD para estimativa precisa da força do vento sobre as estruturas com alturas baixas foi explicada. Para a validação das condições de fronteira realizamos uma análise do escoamento em toprno de um edifício baixo TTU e comparámos os nossos resultados com resultados experimentais e outros estudos numéricos. Mostra-se que um dado conjunto de condições de fronteira resulta numa aproximação razoável do campo de pressão em torno do edifício. Usando o mesmo conjunto de condições de fronteira simulou-se um fluxo sobre o guarda-sol com $Re = 3 \times 10^6$ com $14,5\%$ de turbulência na altura do guarda-sol. Mostramos que a solução RANS estado estacionário é comparável com situações não estacionárias, o que essencialmente significa que o fluxo é constante no sentido estatístico e não há vórtices dependentes do tempo, como encontrados em corpos com cantos. Nove ângulos de incidência do vento diferentes são simulados a partir de 0^o a 240^o com intervalo de 30^o para identificar o cenário de carga extrema. Os resultados mostram que a carga extrema é sentida ângulos de 0^o e 30^o enquanto que as restantes cargas estão entre estas duas. Portanto, a análise CFD é realizada em escala completa a 0^o e 30^o para que o campo de pressão gerado possa ser facilmente usado para definir cargas estruturais. Áreas médias ponderadas de pressão em cinco sub-regiões do guarda-sol são calculadas e são usadas para verificar a integridade estrutural. Em seguida, realizamos uma análise FE em dois tipos de projeto usando composto de fibra de vidro e alumínio industrial. Os resultados demonstraram que o composto não é adequado para a corrente aplicação. Sem qualquer estrutura interna (reforços), o composto com espessura combinada de $5,4$ milímetros sofre uma deflexão de $26,10$ mm na ponta do guarda-sol. Considerando um projeto com tubos de alumínio com uma secção transversal de $20mm \times 20mm \times 2mm$, o desvio é de apenas $2,4$ mm, que está na faixa prática de von-Mises de 10.4MPa dando ao projeto um fator de segurança de $1,92$. Além disso, o peso resultante do alumínio é $9,07$ kg em comparação com $55,78$ kg, no caso de compósito. Portanto, um projeto metálico promete uma solução leve e barata para o guarda-sol em estudo e será seguido para o fabrico.

Contents

Appendix A Log files for Structural simulation **A-1**

List of Figures

List of Tables

Abbreviations

EFM Environmental Fluid Dynamics

ABL Atmospheric Boundary Layer

CFD Computational Fluid Dynamics

RANS Reynolds Average Navier Stokes Equations

TTU Texas Tech University

LES Large Eddy Simulation

AIJ Architecture Institute of Japan

COST European Cooperation in Scientific and Technical Research

FSI Fluid Structure Interaction

ASCE American Society of Civil Engineers

FEM Finite Element Method

FEA Finite Element Analysis

List of Symbols

l_t- Turbulence mixing length
u_*- Frictional velocity
z- Height above the ground
z_o- Aerodynamic roughness length
κ- von-Karman constant
K- Turbulent kinetic energy
ϵ- Turbulent eddy viscosity dissipation
C_μ- Model constant of standard $k-\epsilon$ turbulence model
u,$\bar{u}$- Mean velocity in horizontal direction
U_H, U_{ref}- Reference wind speed at the height of object
γ- Exponent of power law
ρ- Fluid density
ν- Fluid kinematic viscosity
μ- Fluid dynamic viscosity
Re- Reynolds number
t^*- Non dimensional time
K_s- Equivalent sand grain roughness
μ_T- Turbulent viscosity
I- Turbulene intensity
C_P- Mean pressure coefficient
$C_{P,U}$- Mean pressure coefficient at upper surface of sunshade
$C_{P,L}$- Mean pressure coefficient at lower surface of sunshade
L- Chord length of sunshade
α- Wind incidence angle
P_{av}- Area weighted average of pressure
E- Young's Modulus
G- Shear Modulus
ϑ- Poisson's ratio
σ_t- Ultimate strength of composite in tension
σ_c- Ultimate strength of composite in compression
ρ_{comp}- Density of composite

1

Introduction

Contents

1.1 Introduction

Numerical analysis has become an essential part of the product development cycle as it allows designers to understand effects of various parameters on the design output. Advancements in computational power has enabled researchers and designers to model and simulate complex systems for design optimization before actual physical system is in place. Current work is also being carried out as a part of product development of a small startup struggle. The company follows the ideology of integrating sun power in daily commodities which will serve the long time purpose of changing attitudes of people. Founding idea is a result of market survey which gauged perception of conventional photovoltaic modules for roof top applications and result suggested that a big majority does not opt for this solution solely because of aesthetic reasons. Goal is to offer green solutions serving aesthetic need of customers along with clean energy.

1.2 Motivation

To enter the market, we decided to offer a solar integrated sunshade (parasol), a shadow space addressing beaches, hotels and individual opinion leaders as target groups. Having their basic needs fulfilled this product would offer differentiation as a key value proposition to our customers. Following the current macro trends, a product of such an exclusivity offering improvement in green profile promises a business opportunity worth to take risk and validated. Business plan for the company has been written and validated during an internship in lieu of current master thesis at KIC InnoEnergy Business Incubator Barcelona, Spain. Main achievements while writing business plan were to define a niche market for the proposed solution and validation of business model through detailed interviews conducted at Mykonos Island, Greece from luxury hotels owners. Interviews supported our assumption of need in hospitality sector for a solar integrated parasol or sunshade. Hospitality sector is well known to its negative contributions to the environment and has been a culprit for long time. Therefore this sector is actively seeking for solutions that are environmental friendly as well as contributing positive towards clients comfort. During conducted interviews, a commonly shared concern was related to the strength of the conventional umbrellas (detailed interviews are presented in Part I: Business Plan) during windy weather of Island. To fulfill this requirement, proposed solution has to withstand such wind conditions. This has lead us to investigate the wind forces on designed sunshade that can be ultimately used for structural integrity verification. Designed sunshade can be seen in Fig.1.1 where a small solar module is attached on top to provide ample energy for charging hand held devices.

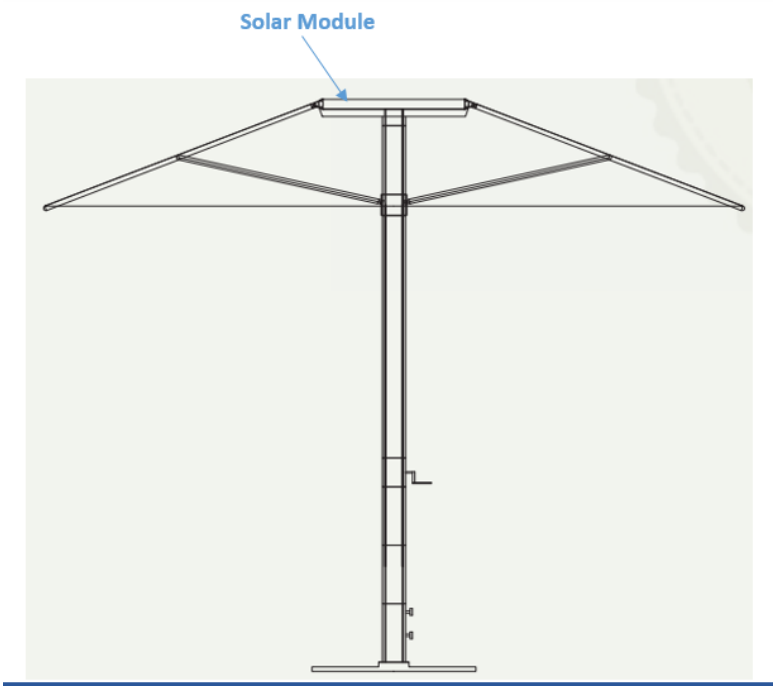

Figure 1.1: An example of solar integrated sunshade design.

Product functionality and customer satisfaction make verification and validation an essential part of engineering design [5]. After abstraction of idea into tentative design, next phase involves digital modeling employment and computational design and simulations. Experimental verification procedures have their due importance mainly to support numerical results, however current industry practices clearly are moving towards virtual testing and verification. Thus as a part of product development, we perform computational study for a wind resistant design.

1.3 Literature Review

To estimate the wind forces correctly it is necessary to review numerical studies for flow physics of the lower portion of the atmosphere where all the low rise structures interact with wind. Computational studies to understand the effect of turbulent Atmospheric Boundary Layer (ABL) are multidisciplinary ranging from pollutant dispersion modeling to pressure loadings on low rise structures. Mathews [6] predicted the wind generated pressure distribution around a building for natural ventilation studies and concluded that extension of his work can simulate flow around complex buildings. While commenting on his work, Richards and Younis [7] pointed out inconsistencies in turbulence model and inflow boundary condition equations. They argued that defining inflow velocity profile using empirical power law is not coherent with turbulent model and this results in degradation of flow throughout the domain. Due to this degradation actual intended flow properties do not reach near the point of interest in computational domain that raises a question on the results. Later Richards and Hoxey [8] presented consistent set of boundary conditions for fully developed neutral ABL where horizontal velocity profile is given by log law instead of empirical power law. Their inflow profiles of velocity, turbulent kinetic energy and eddy dissipation rate were consistent with standard $k - \epsilon$ model and

showed no degradation of flow in computational domain. Since then these set of inflow conditions have been used by numerous researchers [9] investigating flows inside neutral ABL using RANS turbulence models. However researchers have reported various difficulties while implementing profiles suggested by [8]. Zhang [10] reported an unwanted change in mean wind profile and especially turbulent kinetic energy using standard $k-\epsilon$ model and standard wall functions to resolve the boundary layer near the ground. While simulating flow on a backward facing step, he argued that such numerical errors can give rise to serious errors in the pressure and velocity estimations.

Standard $k-\epsilon$ model inherits serious shortcomings of over estimating pressure loadings on the flow impinging walls as discussed by Tsuchiya et. al [11]. To overcome this issue, authors investigated flow past 2D rib, cube and a low rise building model by a modified standard $k-\epsilon$ (LK) model and a newly developed $k-\epsilon$ (MMK) model. They showed that results behind bluff body are better predicted using their turbulence models compared to standard $k-\epsilon$, however deficiencies still remained compared to experimental results. Working group from Architecture Institute of Japan (AIJ) during a workshop organized for flow around high rise building noticed that standard $k-\epsilon$ model is incapable of reproducing the experimentally observed reverse flow on the roof top where all modified $k-\epsilon$ models do not exhibit this problem [12]. Walshe [13] while utilizing consistent set of boundary conditions for $k-\epsilon$ model by [8] for simulating ABL flow over a complex terrain noticed an unexpected spike of turbulent kinetic energy at the node adjacent to ground boundary. He associated this peak as a peculiar property of $k-\epsilon$ turbulence models. Riddle et. al [14] also observed the same issue while implementing neutral ABL in Fluent and ADMS softwares. This problem has been clarified in [15] where authors have shown that this anomaly is not an inconsistency of turbulent models rather its a discritization error of ANSYS software that can be solved if program utilizes face centered schemes rather than cell centered near the ground boundary.

Problems associated with implementation of consistent set of boundary conditions in commercial codes of both CFX and Fluent are also discussed by Hargreaves and Wright [16]. They provided the remedy of degrading profiles through the computational domain by applying a constant shear stress at the top boundary of domain. Note that this condition was already mentioned by Richards and Hoxey [8], however its implementation in commercial codes was not easy and therefore ignored by many authors, see for example [14, 17]. Authors also suggested that laws of walls near the ground boundary should be modified in commercial codes for rough walls for correct neutral ABL simulation. In a systematic approach to understand the effect of improper modeling of boundary conditions in commercial codes, Sullivan et. al [18] showed that inconsistent top boundary layer causes most erroneous results causing streamwise gradients of velocity and turbulence profiles. Use of inconsistent top boundary condition resulted in an artificial increase of 4% in velocity within height of $150m$ ABL which may cause 12.5% increase in estimated power for windfarm potential studies.

As modeling of neutral ABL is vital to various engineering fields therefore a required guide to implement boundary conditions proposed by Richards and Hoxey [8] in CFX and Fluent was first presented by Blocken [3]. A common practice to report the field surface roughness for ABL is to specify aerodynamic roughness length as done by [19] whereas CFX and Fluent define rough wall

(required for ground boundary) using an equivalent sand grain roughness. This sand grain roughness is further utilized by wall functions for resolving boundary layer near the ground by software. Blocken presented relationship between aerodynamic roughness and sand grain roughness for Fluent and CFX both which helped him to get a stratified neutral ABL.

Yang et. al [20] discussed the problem associated with constant kinetic energy profile at the inlet proposed by Richards and Hoxey [8] as this is not the case in wind tunnel and field data where observed values are much higher. They emphasized that modifications presented by Hargreaves and Wright [16] results in limited improvements and extra errors occurred elsewhere in the domain. Authors presented a modified inflow profile for turbulent kinetic energy which varies with height to incorporate vertical gradient observed in real conditions. Another modification of turbulent kinetic energy profile equation has also been discussed by Gorle et. al [21] for environmental pollutant modeling. They used turbulent kinetic energy equation proposed by Yang. et al [20] and modified various constants of $k-\epsilon$ model to be consistent with turbulence model. They showed that 40% lower turbulent kinetic energy in case of constant profile results in 90% higher prediction of maximum concentration near the source. Later Parente et. al [22] suggested modifications to the wall function in Fluent using user defined functions such that production of turbulent kinetic energy is not integrated at the cell height adjacent to the ground wall rather is done at centroid which mitigated the issue of spike at ground adjacent node reported by various previous studies discussed. This allowed authors to have a dense mesh near the ground wall which otherwise is not possible as height of the first cell is limited by standard wall function approach in commercial codes [3]. They also added two source terms in turbulent kinetic energy equation to ensure consistency. In an application to low rise buildings Kose et. al [23] incorporated wind tunnel profile of turbulent kinetic energy that resulted in big streamwise gradients. Intensity was reduced till the time they successfully achieve neutral ABL. Despite of low turbulence used, results produced good agreements of mean pressure coefficient over buildings. However such remedies are case dependent and can't be generalized.

Later Richards and Hoxey [15] revisited their consistent inflow conditions for $k-\epsilon$ model considering numerous difficulties for application to commercial codes by various authors. They presented implementation of homogeneous ABL in CFX with a number of eddy viscosity models along with a Reynolds stress model (QI) and showed that to avoid over estimations in computational engineering problems, Reynolds stress models should be further explored in case of Reynolds Average Navier Stokes Equations (RANS) modeling. To incorporate field turbulent kinetic energy profiles at the inlet, Balogh et. al [24] modified law of wall in Fluent and OpenFoam, as well as modified the default constants for the RNG $k-\epsilon$ model to achieve consistency. Results from OpenFoam showed better accuracy in velocity profiles while real levels of turbulent kinetic energy were achieved using modifications in Fluent. A recent study by Jureti'c and Kozmar [25] showed that with modification of standard $k-\epsilon$ equations using Reynolds stresses in computational domain leads to consistency throughout the domain. This study showed a novel approach to incorporate vertical gradient of turbulent kinetic energy while maintaining profiles, however is not focused on commercial codes.

To perform authentic modeling and analysis Jakeman et al.[26] pointed out ten iterative steps. Steps

outlined in the study are general in nature and can be extended to computational wind engineering domain. Authors noticed that most of the modeling is done without a clear objective, therefore defining objective and refining it with the availability of missing data and clarity of implementation is essential. Best practices should also be considered for respective context in order to extract maximum data required for reliable modeling. Model should then be validated and quantification of uncertainity must also be considered. Performing all these steps would lead to actual model evaluation or testing for required application. In Environmental Fluid Dynamics (EFM) computational community Franke [27] presented such guidelines to perform urban environment flows. His work was result of four years of literature review in computational wind engineering. Author outlines numerous rules including domain size, turbulence model selection, mesh sensitivity and model validation. He concludes not to use standard $k-\epsilon$ model rather revised versions should be first choice for RANS simulations. Similar guideline was outlined by AIJ [28] which follows rules laid out by Franke [27]. Authors here also do not recommend to use standard $k-\epsilon$ model due to over estimation of turbulent kinetic energy near the building or structure that will lead erroneous results. Working group of AIJ also outlines comparable steps for estimating pressure loads on buildings using Computational Fluid Dynamics (CFD) [29]. They showed that mean pressure distribution around buildings can be reproduced within acceptable levels to experimental and wind tunnel results using steady state RANS simulations. All the guidelines recommend to use Large Eddy Simulation (LES), however they acknowledge the computational cost associated to it that makes it unfeasible for most of engineering problems. Another set of guidelines developed for EFM by Blocken and Gualteiri [30] details ten iterative steps necessary to estimate particle mixing and flow dispersion. Authors implemented recommendations on transverse turbulent mixing in shallow water flow and urban flow for indoor ventilation in case of Amsterdam ArenA football stadium. Both cases were chosen to show the applicability of proposed steps to simple as well as complex flows.

Computational wind engineering models have also been used to study forces on structures other than buildings placed within the ABL. A detailed review for the application of CFD in computational wind engineering has been provided by Aly [9]. Author discusses state of the art in wind tunnel and computational modeling for wind engineering and also discusses the current limitations associated with each study. Simulation models for ABL are complex either by wind tunnel or using CFD where matching one parameter to full scale or field values might result in distortion of others. Author shares the idea of Richards and Hoxey [15] that much of the focus has been put in the past to match all of the parameters with field studies which has not lead to any clear roadmap and therefore encourages to develop new rules where out of box thinking in context of ABL simulation is required. He explained two methods of turbulence generation at inlet for LES studies namely smooth inflow where uniform velocity corresponding to building height is applied and fully turbulent where all small scales of turbulence are also modeled. Comparison revealed that ratio of peak pressure coefficients generated does not deviate much from one and hence any method can be pursued. In his earlier study [31], author performed wind tunnel and computational modeling to find pressure loadings on ground mounted solar panels placed in ABL. Scaled wind tunnel experiments and CFD to mimic these test conditions were performed

using LES. He concludes that mean pressure coefficients on low rise structures do not change with model scale and neither with turbulence content in the incoming flow.

Wind flow characteristics for a solar panel attached on roof top of a low rise building is studied by Pratt and Kopp [32] using atmospheric boundary layer wind tunnel. They concluded that interaction of ABL with small architectural features should be considered as in case of studies where roof mounted PV arrays are not modeled above buildings will not yield correct peak uplifts. Small inclination angle of solar panels with respect to incoming wind did not change flow field and primary vortex causes uplift on the rooftop whereas for large tilt angles (20^o in this case) separation and reattachment near the solar panel caused uplift. Another experimental study performed in ABL wind tunnel of Concordia university, Canada for investigating wind loads on roof mounted as well as stand alone solar panels is presented by Stathopoulos et. al [33]. A $1:200$ scaled model studies showed that extreme loadings occur at the an azimuth (wind incidence angle) of 135^o. Effects of building height, location of the panel on the rooftop and inclination were also studied and they found out that peak maximum pressure coefficient does not change with the inclination of the solar panel varied from 0^o to 45^o. Their study was aimed to help verify the Australian code for loading calculations and found out that it is in good agreement. Shademan and Hangan [34] conducted a numerical study to estimate the wind force coefficients on stand alone and arrayed ground mounted solar panels. They used empirical power law with maximum speed as provided in ASCE07 [35] with turbulence intensity of 16% at the inlet and provided values of force coefficients that can be used in design of such configurations. Later a wind tunnel and computational study is carried out on a single and array mounted configurations of solar panels by Bitsuamlak et.al [36]. They used LES for turbulence modeling and found out that CFD underpredicted the wind loads in general in four different cases of angle of attack variation.

Discrepancies in wind load estimations in various codes worldwide for free standing canopy roofs lead a research at Oxford where Gumley [37] conducted a parametric wind tunnel study to understand the effect of various parameters on mean and peak pressure loadings. He performed all his experiments with a velocity profile of rural terrain ($z_o = 30mm$). Results showed that UK code for wind loading used at that time underestimated wind loading for such structures and therefore may lead to design failures. Later Ginger and Letchford [38–40] conducted wind tunnel experiments on $1:100$ scaled model of free standing canopy roof with terrain surface roughness ($z_o = 20mm$) and found out that worst loading scenario is depicted at wind incidence angle of 30^o where corner promotes flow separation leading to a delta wing vortex. Mean pressure loadings in suction region were slightly lower than experiments of Gumley [37] and authors associated this to mainly higher turbulence modeled in their study compared to the previous one. On a comparison of Japan building code and previous wind tunnel studies conducted on free standing canopy roofs, Uematsu and Stathopoulos [41] found that Japanese building code also underestimates positive wind forces experienced by leeward half of the canopy which is evident from experimental studies and therefore advised an updated code. To overcome the deficiency in available data authors conducted their own wind tunnel studies on free standing canopies in monosloped, duo pitched and gabled configurations [42, 43]. They found out that experimental results are in good agreement with Australian building code for mono sloped roofs, however show

considerable increase in gable and troughed roofs.

In a recent experimental and numerical study conducted by Poitevin et. al [44], authors demonstrated the incapability of ASCE07 code [35]for estimation of wind loading on open canopy structures with parapets and stated that ASCE07 recommendations are not sufficient to carry out the safe design of such structures. Another purpose of the study was to investigate the capability of computational modeling so that in future studies it could be used as a replacement of wind tunnel studies. Authors used a computational domain that included all the roughness elements in actual wind tunnel to generate experimental turbulence profile before the open canopy structure and showed that mean pressure coefficients are well predicted with CFD and hence it can be used in future investigations with confidence.

Pressure field loading on a metallic roof of $6m$ height is conducted by Diaz. et al. [45, 46] where authors utilize finite element and finite volume methods to estimate the wind loads. Purpose of the study was to generate numerical pressure distribution that can be applied to study the structural response of metallic roof. Design of wind surfer sail was studied by Blicblau et. al.[47] where static structural analysis is carried out against constant wind pressure of 65Pa on one side of the sail. Two potential materials woven polyester and single layer polyester resin for the sail cloth were explored and Finite Element Analysis (FEA) results showed that woven polyester cloth is able to deflect and strain more than the other alternative. They also showed that resulting stresses in the center line of the sail in case of polyester resin cloth are higher. A detailed literature review to estimate wind loadings on an agricultural net is conducted by Briassoulis et. al [48]. They propose a methodology to integrate these wind loadings in structural analysis to achieve low cost optimised structures. Nets are modeled as orthotropic membranes and analyzed using Finite Element Method (FEM). Uniform pressure loads were applied on the orthotropic nets and results on the accompanied structure were detailed. Authors conclude that design criteria requires a change in EU standard for green house system to include net supporting structures.

To understand the dynamic interaction of wind and installed solar arrays Schell et. al. [49] performs non linear wind response history analysis. Motivation of the work was to analyze the current static structural analysis practices prevailed in industry. Experimentally observed dynamic wind data was used to analyze the transient structural response of solar array and it has been concluded that current codes of static structural analysis are appropriate design tool defining wind loads and required strength of structural members. A thin membrane structure of $29m$ span umbrella has been analyzed using coupled fluid structure interaction by Michalski et. al [50, 51]. Mean wind flow characteristics were observed in a full scale experimental facility in Germany for one complete year. LES was then utilized to model neutral atmospheric boundary layer representing observed velocity and turbulence at the height of umbrella. Computational structural dynamics results showed a variation of $\pm 25\%$ in deflections observed at experimental facility. It was an industrial project performed to set standards for computational coupled models for thin structures design. Computational model overall showed a reliable agreement with experimental study.

1.4 Objectives

The objective of present thesis is to design a wind resistant solar sunshade as a part of product development cycle. Whole study is carried out with an aim to generate good enough estimation of wind forces in computational regards. However due to limited computational resources as well as expertise in softwares utilized, certain compromises have been made while maintaining the fulfillment of defined objective. In certain cases where computational results are ambiguous, we choose conservative results such that overall objective of structural integrity is served. Objective has been achieved in three steps which are listed below.

1. A detailed literature review is conducted to analyze the best computational practices in wind engineering. This helped in achieving appropriate boundary conditions required to simulate neutral atmospheric boundary layer. To validate deduced set of boundary conditions, we compare our computational results of pressure field over Texas Tech University (TTU) building with experimental, field as well as numerical studies conducted earlier. Results show good agreement.

2. Wind flow analysis is performed using CFD. This results in a detailed flow field around the object of interest which in our case is solar sunshade. Loading is then extracted from flow by area weighted average of pressure field at various sub regions of sunshade.

3. We then use pressure loading to analyze structural integrity of solar sunshade. Design with two different materials is analyzed. Based on the resulting material deflections and stresses, metallic design is found to be superior than composite material design.

1.5 Outline of Thesis

1. A general introduction to the problem and motivation to conduct the study are presented in Chapter 1. Detailed literature review of computational wind engineering as well as structural anlayses is also presented. Furthermore we also define objectives and their systematic accomplishment.

2. Physics of lower part of atmosphere is discussed in Chapter 2. Since current work is of computational nature, therefore application of neutral ABL in wind engineering is further presented. Consistent set of boundary conditions are deduced from literature review and are validated by comparing pressure field on the roof top of TTU building to that of experimental and other numerical studies.

3. In Chapter 3, we perform CFD simulations to generate pressure and velocity fields around the solar sunshade. We also investigate extreme loading scenario by simulating wind flow from 9 different directions. Then we perform full scale study to extract pressure to carry our structure integrity analysis.

4. Static structural analysis of sunshade under wind loading is discussed in Chapter 4. We present mesh independence and different materials analyzed for the design. An iterative methodology to

reach meaninful results is also explained.

5. We summarize and conclude the conducted work in Chapter 5. Limitations of the current work and recommendations for future work are presented.

2

Neutral Atmospheric Boundary Layer

Contents

2.1 Introduction

The lower portion of the atmosphere is vital to mankind as we live and breath in it. Concept of boundary layer where fluid interacts with solid was first described in 1904 by *Ludwig Prandtl*. He explained that moving fluid can be divided into two regions- a bulk of fluid where effect of viscosity could be neglected and boundary layer where fluid interacts with solid and viscosity plays an important role. As a result of this viscous interaction tangential velocity of the fluid becomes zero at the surface of solid. This became the basis to understand aerodynamic drag and lead to successful design of aircrafts and ultimately manned flight.

In EFM, lower portion of atmosphere also known as ABL is particularly important as it helps to understand particle dispersion [52–56], gaseous discharges [57–60], natural ventilation [61, 62], wind driven rains [63–65] , wind erosion [66, 67] and wind engineering [68–71] to name a few. Understanding flow physics within this ABL is therefore vital in discipline of EFM. Thickness of ABL depends on the surface roughness as well as diurnal cycle. According to Kaimal and Finnigan [1] ABL is the lowest 1-2 km of the atmosphere, a region influenced by exchange of momentum, heat and water vapour at the earth's surface. On a clear day it can be divided into three layers as shown in 2.1.

1. *Frictional sublayer* which is affected by the friction of individual elements such as grass, water, trees and buildings
2. *Surface layer* that usually is 100-200m thick or 10% of the ABL where wind velocity, temperature and humidity vary rapidly with altitude and turbulence characteristics depend on surface roughness. However vertical fluxes of heat and momentum are constant
3. *Well mixed layer* where effect of earth's rotation become significant and resulting temperature and humidity stays constant whereas wind speed continues to increase
4. *Capping Inversion* Due to sudden change of wind, temperature and humidity this layer acts as a capping which inhibits turbulent mixing causing air pollution to be trapped inside ABL.

During night time velocity profile within these sub layers change considerably because of less temperatures at the surface of earth.

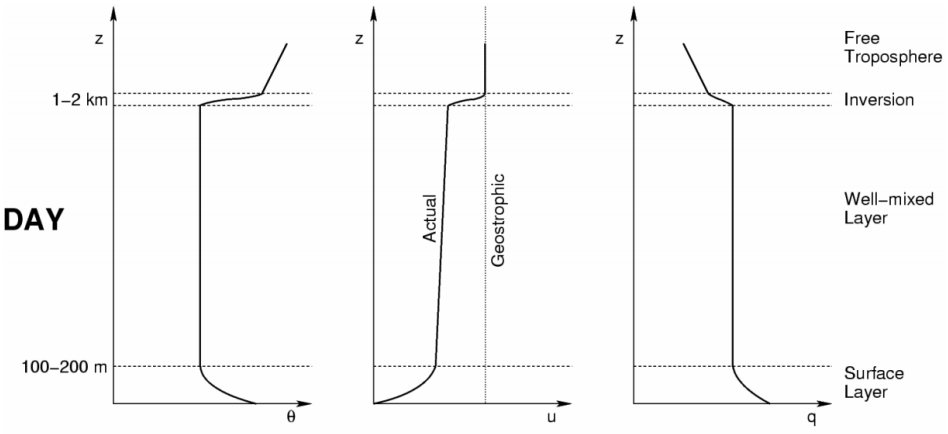

Figure 2.1: Typical profile of temperature, wind and humidity over land in midaltitudes in cloudless conditions [1].

In ABL flow, turbulence occurs due to mean wind shear ($\frac{\partial \bar{u}}{\partial z}$) and temperature variation. In a neutral thermal surface layer, turbulence by mean wind shear is much larger than buoyant production or suppression (due to absence of temperature stratification) [72] and therefore turbulent mixing length (l_t) is only proportional to the height above the surface (z) as given by eq.2.1. Such a boundary layer is known as neutral ABL.

$$l_t = \kappa z \tag{2.1}$$

Whereas in turbulent mixing theory proposed by Prandtl, turbulent mixing length is associated with frictional velocity (u_*) and mean wind shear by following equation [1, 72],

$$u_* = l_t \frac{\partial \bar{u}}{\partial z} \tag{2.2}$$

Frictional velocity u_* stays constant with the height as found out by experimental measures therefore by rearranging and integrating eq.2.7, we obtain the following log law which governs mean wind speed in neutral ABL.

$$\bar{u}(z) = \frac{u_*}{\kappa} \ln\left(\frac{z}{z_o}\right) \tag{2.3}$$

where z is the height above the ground, z_o is aerodynamic roughness length where mean velocity of the fluid becomes zero at the surface of the object and κ is von-Karman constant that has a value of around 0.4 derived from experiments and it slightly varies to this value in all turbulent flows. Aerodynamic roughness length (z_o) is a measure of terrain surface roughness and varies from 0.001m at the surface of ice or water to several meters over urban areas [73].

2.2 CFD Modeling of Neutral ABL

In addition to the traditional investigation methods like analytical modeling and experimental testing, CFD has evolved as an integral part of problem solving in wind engineering discipline. With the advent of computational capabilities, mathematical modeling has helped us understand the flow physics of various natural occuring flows in detail by use of partial differential equations, numerical models to solve analytical complex equations and also by means of commercial codes that involve pre-processing, solution and post processing capabilities [9]. CFD has advantages that flow field in all the computational domain can be estimated compared to wind tunnel testing where data at certain sensor locations is usually measured [74]. Interaction of wind with structures causes forces that may be used as an advantage in case of wind energy but could also pose a threat for built environment. Taconama Bridge collapse on November 07, 1940 is one such notorious case where wind has caused severe damage as shown in 2.2. In lieu of all these potential effects, numerous studies have been published to estimate wind loading on low and high rise buildings [7, 23, 75, 76].

Figure 2.2: Taconama bridge collapse in 1940. Photo taken by Barney Elliot, produced here according to fair use principles; [2]

As all of these wind interactions occur in the lower atmosphere layer, therefore it is essential to model neutral ABL accurately in the computational studies to get reliable results [18, 27, 77]. In computational wind engineering studies, it is recommended to obtain the wind characteristics data from on site measurement where possible and apply fully developed neutral ABL wind velocity and turbulence profiles at the inlet of computational domain [74]. However, application of developed profiles at the inlet results in an undesired decay of velocity and turbulent intensity profiles at the point of interest within computational domain (e.g. building, structure) compared to the ones specified at the inlet [20–22]. This issue of having unintended streamwise gradients of velocity and turbulence profiles through computational domain is known as horizontal homogeneity problem. Existence of these streamwise gradients is a direct consequence of inconsistencies between fully developed ABL profile and wall function formulation of commercial CFD codes [22].

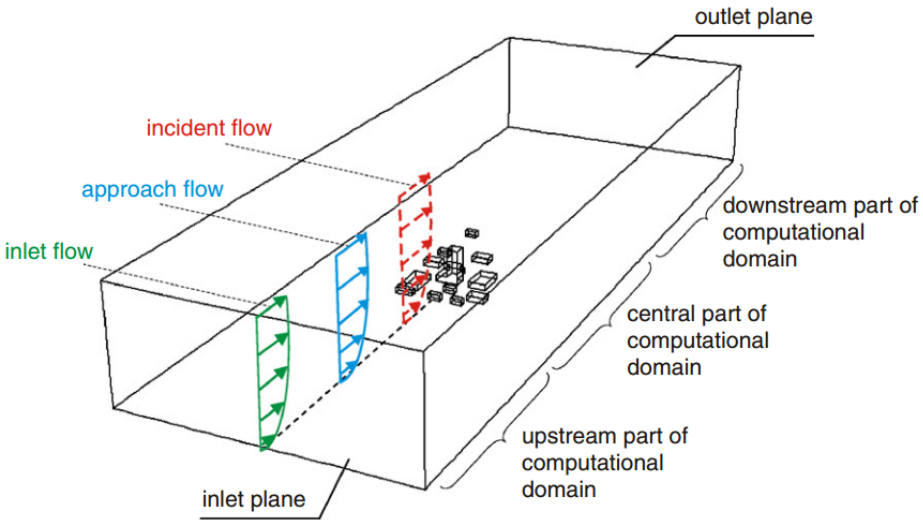

Figure 2.3: Computational domain with building models for CFD simulation of ABL flow: definition of inlet flow, approach flow and incident flow and indication of different parts in the domain for roughness modeling, reproduced from [3]

Richards [7] noticed the issue of horizontal homogeneity in the work of Mathews [6] for predicting wind generated pressure around buildings. Richards pointed out that use of empirical relations to define

inlet boundary conditions resulted in vertical velocity that is not self sustaining. Later in [8], Richards and Hoxey proposed consistent boundary conditions that would result in horizontal homogeneous neutral ABL for $k-\epsilon$ turbulent model as follows:

Horizontal Velocity Equation

$$\bar{u}(z) = \frac{u_*}{\kappa} \ln\left(\frac{z}{z_o} + 1\right) \tag{2.4}$$

Turbulent Kinetic Energy Equation

$$K(z) = \frac{{u_*}^2}{\sqrt{C_\mu}} \tag{2.5}$$

Eddy Viscocity Dissipation Equation

$$\epsilon(z) = \frac{{u_*}^3}{\kappa(z + z_o)} \tag{2.6}$$

Frictional Velocity Equation

$$u_* = \frac{\kappa \bar{U_H}}{\ln\left(\frac{H}{z_o} + 1\right)} \tag{2.7}$$

where K(z) and $\epsilon(z)$ are turbulent kinetic energy and eddy viscosity profiles and C_μ is a model constant having a value of 0.09 taken from [8]. Values of κ can be found for each variation of eddy viscosity models in [15] which in general stays between 0.41 to 0.433. $\bar{U_H}$ is the horizontal mean velocity at height of the object H (z=H). Zhang [10] using $k-\epsilon$ turbulent model and standard wall function reported an unwanted change in mean velocity and turbulent intensity profiles which he suggested were the reasons for discrepancies in CFD and wind tunnel data. Importance of incident profiles on the CFD results around buildings has also been discussed in [65, 75, 76]. Nearly after two decades since first presented by [8], horizontal homogeneity is still an issue to be addressed in CFD studies of neutral ABL in EFM. As nowadays commercial codes are usually used for engineering estimates, therefore implementation of consistent boundary conditions by [8] in these softwares needs to be addressed. Riddle et. al [14] has compared Fluent and ADMS softwares for flow dispersion modeling using $k-\epsilon$ model. They maintained the inlet mean velocity and turbulence profiles fairly well till the height of 800m, however wind shear increased with distance of lower 50-60m of ABL. Hargreaves and Wright [16] state that inflow boundary conditions proposed by [8] are necessary but not sufficient for modeling neutral ABL and therefore proposed modifications in ground and top boundaries of computational domain. A comprehensive guide to achieve horizontal homogeneity is first presented by [3]. Author describes that incident profiles of mean velocity and turbulence are fully developed and these profiles should be representative of roughness characteristics of the part of the upstream terrain that is not included in the computational domain by either specifying appropriate aerodynamic roughness length (z_o) or appropriate power law exponent (γ) of the terrain in the expressions of inlet profiles. He successfully applied all the consistent boundary conditions given by eq. 2.4 to eq. 2.7 in ANSYS CFX and Fluent by modifying constants in law of wall of these softwares.

An issue with inlet boundary conditions proposed by Richards and Hoxey [8] is a constant turbulent kinetic energy profile given by 2.5 which is not the case in wind tunnel testing and on site data measurement [21]. Therefore various authors while modeling neutral ABL for different applications have associated discrepancies in numerical and wind tunnel results with improper modeling of neutral ABL in CFD codes using RANS [55, 58, 59].

2.3 Validation Study- Texas Tech University Building

In a CFD study, computational results are often compared with on site data measurement which is not the case always, therefore wind tunnel simulations are carried out on scaled models to validate the computational estimations. In a design case where neither full scale nor model scale data is available, high quality data sets already published in literature should be used for validation studies [74]. Therefore in this section we validate numerical model settings and boundary conditions essential to simulate neutral ABL correctly and estimation of wind mean pressure over a low rise building which in our case is TTU buidling immersed in a turbulent neutral ABL is presented.

Most of the built structures around the world for residential, commercial and other purposes can be categorized as low rise buildings [78]. Wind loads on these buildings can cause significant damage [9], therefore it has been a hot research topic since early 90s. To estimate the pressure loadings as a result of wind interaction, several wind tunnel facilities were developed e.g. [79, 80]. One such experimental facility is TTU building located at Wind Engineering Research Field Laboratory (WERFL) in the high planes of Lubbock, Texas, USA [17]. Building has dimensions (L x B x H) of $9.1m \times 13.7m \times 4.0m$ with almost straight roof top. Building can be rotated allowing for various wind angle of attacks for pressure investigations [78].

Meteorological field data for TTU building, monitored by sensors mounted on 46m high tower near the model building [78] was first reported by Levitan et. al [81, 82]. And pressure over the TTU building was published by [19] a year earlier. Furthermore wind tunnel studies on scaled model were also conducted [80] that helped in improvement for wind tunnel modeling. Earlier computational studies using RANS [83, 84] and LES [85–87] were conducted and results were compared with field data. A recent study by [23] reported results of wind tunnel testing as well as LES computations for flow past TTU building and achieved a very good agreement between experimental and computational results. In general RANS turbulence closure models including standard $k-\epsilon$, RNG $k-\epsilon$ and Kato-Launder $k-\epsilon$ over estimated the mean pressure values at the roof top of building. However reported LES results were in good agreement with the field data.

As LES is computationally expensive, therefore recent studies [17, 18, 22] have employed RANS closure modeling with improved inlet flow profiles presented by Richards and Hoxey [8]. In this study we also employ RANS turbulence models for investigation of flow past TTU building.

2.3.1 Numerical Methodology

The flow in the current problem is governed by the incompressible continuity and momentum (Navier-Stokes) equations, which can be represented as follows:

Continuity Equation

$$\frac{\partial u_i}{\partial x_i} = 0 \tag{2.8}$$

Momentum Equation

$$\frac{\partial u_i}{\partial t} + \frac{\partial}{\partial x_j}(u_j u_i) = -\frac{1}{\rho}\frac{\partial p}{\partial x_i} + \nu\frac{\partial^2 u_i}{\partial x_j \partial x_i}, \tag{2.9}$$

where i,j=1,2,3; the u_i represents the Cartesian velocity components (u,v,w) in longitudinal, lateral and normal directions; p is the pressure; ρ is the fluid density; and ν is the fluid kinematic viscosity. Equations 2.8 and 2.9 are non dimensionalized using height (H) of the building above the surface of the ground as the length scale and freestream velocity (U_{ref}) as velocity scale. Thus Reynolds number is defined by $Re_H = \frac{U_{ref}H}{\nu}$ where $\nu = \frac{\mu}{\rho}$. We employ a structured mesh locally refined near building surfaces. Number of elements are varied in mesh convergence study, however strategy is kept same as shown in Fig. 2.4.

Steady state RANS simulations were used in neutral ABL verification and mesh convergence studies. For turbulence model comparison, unsteady RANS simulations are employed. For discretization of convection term in Navier Stokes equation we use high turbulence scheme available in ANSYS CFX whereas second order backward Euler scheme is used for temporal discretization. Simulation is run for a non dimensional time ($t^* = \frac{tU_{ref}}{H}$) of 15 with non dimensional time step of 0.025. Such timestep is sufficient to resolve necessary flow details. Convergence criteria for each outer loop iteration is set as 1×10^{-4} for all residuals. Results are averaged after initial 20 timesteps. These settings for unsteady RANS are kept same in current work unless otherwise mentioned.

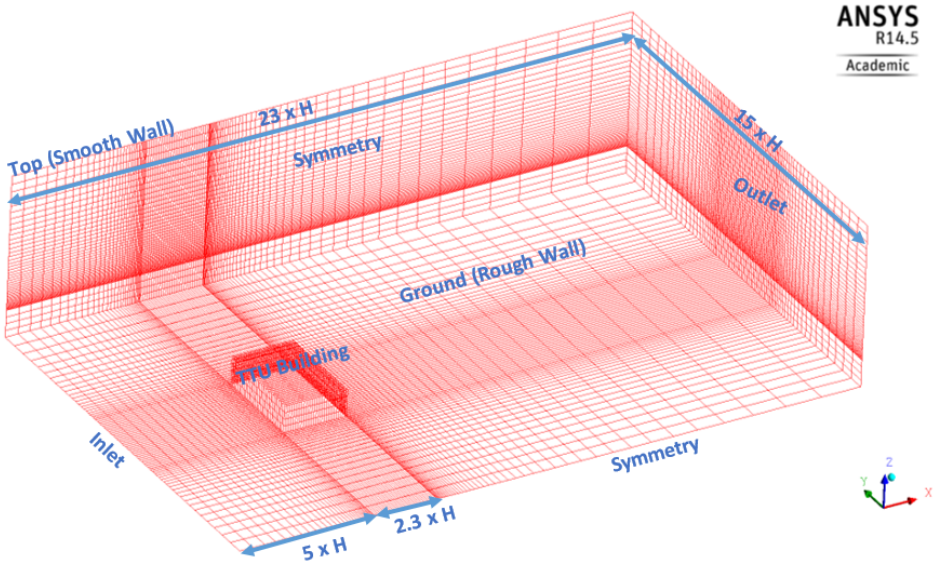

Figure 2.4: Computational domain and mesh strategy for TTU building

2.3.1.A Domain Size and Boundary Conditions

Computational domain is modeled according to recommendations by AIJ [28] and European Co-operation in Scientific and Technical Research (COST) [27, 77], as $23H \times 15H \times 6H$ where $H = 4m$ is the height of the building. To minimize the streamwise gradients or horizontal homogeneity problem, building upstream length should be as minimum as possible (ref). Ref. [17] uses upstream length of $3.85H$ whereas we employ upstream length of $5H$ for proper development of boundary layer. Lateral and top boundaries as suggested by [28] should be atleast 5H away from the target building in each dimension. We use $5.8H$ for lateral boundary on each side of target building and $6H$ for the top boundary. In current work 90° angle of attack is simulated which corresponds to the flow parallel to the short wall ($9.1m$) of TTU building [81, 82]. Therefore normalized dimensions of TTU building

modeled are $2.3H \times 3.4H \times H$ within the flow domain. Downstream length behind the building should be at least $10H$ [27, 28] whereas we use length of $15.7H$.

- *Inlet*: The mean free stream velocity (U_{ref}) recorded in field measurements by [19] is $8 - 10\frac{m}{s}$ and turbulence intensity is $16 - 20\%$ at the building height of $4m$ that translates in Reynolds number (Re) of 2.5×10^6. We simulate $Re = 3 \times 10^6$ based on the dimensionless velocity $\frac{U}{U_{ref}}$ at dimensionless height H of the building. As discussed before RANS closure modeling is used in current study and consistent inlet profiles for $k - \epsilon$ model presented by [8] and revisited in [15] given by eqs. 2.4-2.7 are used at the inlet boundary condition.

- *Ground Boundary*: Representation of building surroundings should be modeled either by using small obstacles upstream of target building or specifying appropriate aerodynamic roughness (z_o) for the ground boundary [28]. Dimensionless aerodynamic roughness for our work is calculated by matching Jenson number ($J = \frac{H}{z_o}$) of 240 from wind tunnel tests [17, 80] to be 4.17×10^{-3}. Alternatively [19] also provides roughness length to be $17mm$ which upon non dimensionalizing by height ($H = 4m$) comes out to be the same. However to model the roughness, wall function approach in CFX which is an extension of the method developed by [88] requires equivalent sand grain roughness (K_s) to be specified instead of z_o [89]. Therefore it is necessary to define a relation between K_s and z_o which according to [20] should be $K_s >= 12.5z_o$. Ref. [16] uses $K_s = 20z_o$ in their work, therefore it varies from code to code. For ANSYS CFX, this can be achieved by first order matching of ABL mean velocity profile with the wall function velocity profile at point 'P' adjacent to the ground wall and is given by $K_s = 29.6z_o$ [3]. Thus no slip boundary condition with dimesionless $K_s = 0.1234$ is set at ground for achieving horizontal homogeneous neutral ABL profiles.

- *TTU Building*: No slip wall boundary condition is given for TTU building which essentially makes flow particles stationary at the surface of building.

- *Outlet*: Relative pressure of 0Pa is applied at the outlet boundary condition for the smooth exit of flow out of domain. This employs that gradients of all flow variables at the exit are 0. Please note that reference pressure of $1atm$ is set for all CFX simulations.

- *Side Walls and Top Wall*: A symmetry boundary condition is employed at the side walls which does not allow flow to exit the domain by setting normal components of the velocity as zero. If the computational domain is large enough then lateral and top wall boundary conditions do not affect the results around the buildings [12, 90], whereas free slip wall (inviscid wall condition) with large computational domain will make computation more stable [28]. Thus top wall is modeled as free slip wall with a constant shear stress of $\rho {u_*}^2$ for homogenous ABL as recommended by [8, 15, 16, 18, 20] where u_* is characteristic velocity given by eq. 2.7. For consistency values of turbulent kinetic energy ($K(z)$) and eddy dissipation rate ($\epsilon(z)$) should be fixed or provided [3]. This can be done by specifying sources of kinetic energy and dissipation in the form of fluxes through top boundary using eq. 2.10 [15].

$$\frac{\mu_T}{\sigma_e}\frac{d\epsilon}{dz} = -\frac{\rho {u_*}^4}{\sigma_e z} \tag{2.10}$$

where σ_e is a model constant with value of 1.1 for standard $k-\epsilon$ model and μ_T is modeled turbulent viscosity calculated at the top of the domain using following relation. Vertical flux for turbulent kinetic energy is set as zero. For analytical understanding of these boundary conditions and model constants, please refer to [15].

$$\mu_T = \frac{\rho {u_*}^4}{\epsilon(z)} \tag{2.11}$$

2.3.2 Neutral ABL

As already discussed, ensuring horizontal homogeneity of inflow velocity and turbulence profiles is vital for computational wind engineering [3, 20]. Therefore boundary conditions discussed in previous section are applied without TTU building inside the domain. Domain is meshed in same strategy (2.4). A structural mesh of $74 \times 52 \times 34$ is employed which gives 123760 hexahedral elements and 144540 nodes. For advection term and temporal discritization, default high resolution scheme available in ANSYS CFX is used. A steady state solution using $k-\epsilon$ turbulence model is run. Convergence criteria for all the residuals is set to be 1×10^{-6}. After reaching convergence, simulation was continued for more iterations till the time there is no significant change in residuals further. Furthermore during the mesh it is considered to place the first cell 'P' above the ground boundary such that $z_P > K_s$ as physically it does not make sense to put first cell into the wall boundary layer [3, 89]. Turbulent intensity is calculated using the eq. 2.12 [18].

$$I = \frac{\sqrt{K(z)}}{\bar{u}(z)} \tag{2.12}$$

wehre $K(z)$ is turbulent kinetic energy and $\bar{u}(z)$ is mean velocity profile. Resultant mean velocity and turbulent intensity profile at inlet, middle and exit of the computational domain are given in Fig.2.5. Note that turbulent intensity at the height of building is slightly less than 16% as provided by [19], however this difference is ignored for the current study.

2.3.3 Results and Discussion

In this section we present the results of the validation study for TTU building. In contrast with the validation of neutral ABL, here we model TTU building inside the computational domain and meshed according to strategy shown in 2.4.

2.3.3.A Mesh Convergence

Three geometrically progressing sets of mesh namely coarse, medium and fine are studied for convergence study. In each mesh, number of divisions are increased almost 50% in all directions with geometric progression of 10% i.e. fine near the building of interest and coarse elsewhere in computational domain as shown in 2.1. Lower portion of the domain till the height of the building is meshed by five divisions (4 elements) in every case fulfilling the requirement ($z_P > K_s$) to avoid

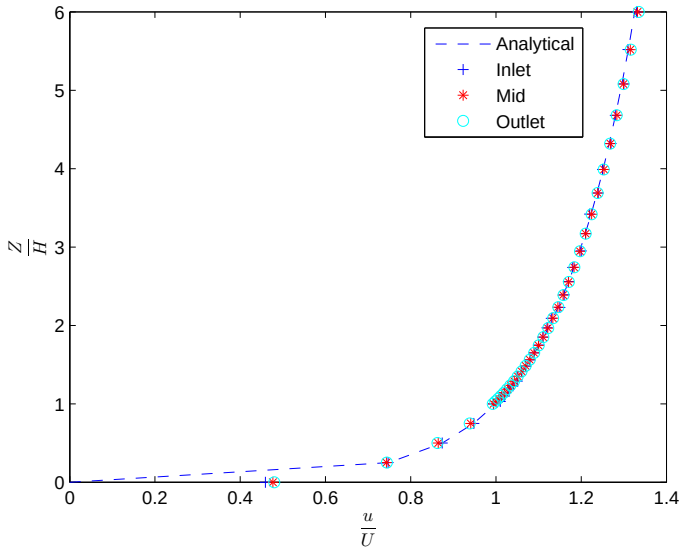

(a) Velocity profile

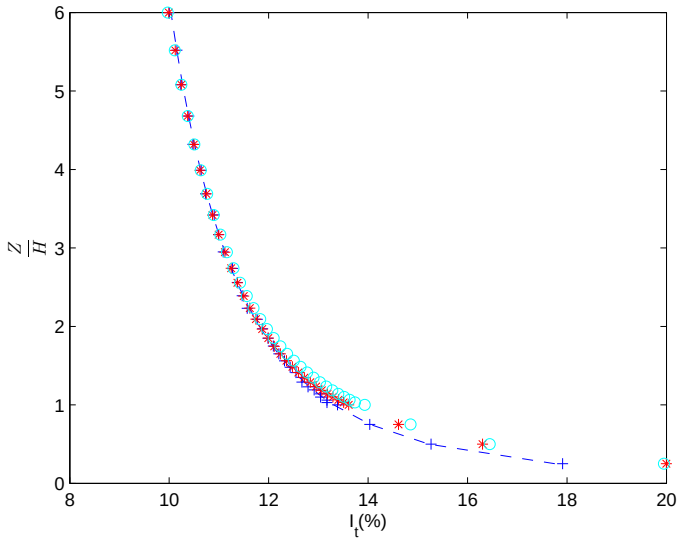

(b) Turbulence profile

Figure 2.5: Validation of boundary conditions for horizontal homogeneous ABL.

streamwise gradients of mean velocity and turbulence profiles [3, 24] as explained in previous section. Increase in number of elements from coarse to medium and medium to fine meshes is 288% and 300% respectively. Steady state RANS simulations were run with rest of the settings same as discussed in previous section.

Mean pressure coefficient calculated using eq.2.13 on the center line of TTU building is presented in Fig.2.6. Since mesh density on the windward and leeward faces is less compared to roof top of the building, therefore we select the mesh size by a focused comparison on the roof. A well known problem of standard $k-\epsilon$ model is its over estimation of near the roof top corner on the windward side [28]. Similar over estimation of the pressure coefficient (C_P) is also reported in [17]. Therefore RNG $k-\epsilon$

Table 2.1: Mesh convergence study for TTU validation study

Mesh	Size	Elements	Nodes
Coarse	$(48 \times 35 \times 24)$	39480	49188
Medium	$(70 \times 52 \times 34)$	122000	142125
Fine	$(105 \times 77 \times 49)$	392205	435370

model is used in mesh convergence study. On the top wall there is practically no difference in the results from medium and fine mesh while coarse mesh results are deviating from field data as well as from medium and coarse meshes. Therefore as a compromise on small improvements in results compared to computational cost Medium mesh settings will be used for further analyses .

$$C_P = \frac{2(P - P_{ref})}{\rho {U_{ref}}^2} \tag{2.13}$$

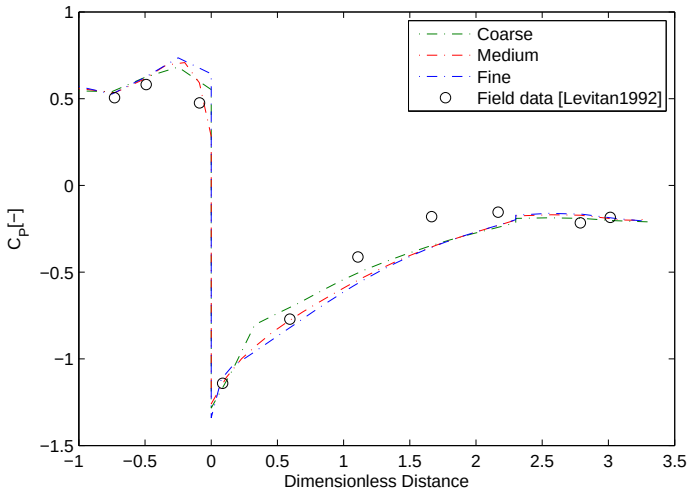

Figure 2.6: Mean pressure coefficient at the centre line of TTU building (parallel to 9.1m wall) with different mesh settings

2.3.3.B Turbulence Model

Another problem of conventional $k-\epsilon$ model is its incapability to reproduce vortex or circulation zone at the roof top due to its over estimation of turbulent kinetic energy at impinging region of the wall [28]. However many revised $k-\epsilon$ models have resolved this issue [12, 90]. COST [27, 77] also doesn't recommend to use conventional $k-\epsilon$ model for wind engineering application. Although [8] presented inflow profiles that are consistent with standard $k-\epsilon$ model for neutral ABL, same profiles can also be used with other RANS turbulence models [3]. Same inflow profiles were used by [15] using LRR QI model and showed that eddy viscosity models may over predict the wind loading on a simple wall normal to the flow in neutral ABL. Therefore it is essential to investigate the effect of turbulence models on the mean pressure coefficient. We use two modified $k-\epsilon$ models namely, RNG-$k-\epsilon$ and $k-\epsilon$ EARSM, and one shear stress model (SST) and results are compared with field data [80], recent wind tunnel study [23] and LES performed by [86]. Unsteady RANS simulations as described in 2.3.1

are performed in all cases and results are averaged after initial 20 timesteps. Mean pressure coefficient C_P is calculated by employing eq. 2.13 at the centre line of TTU building.

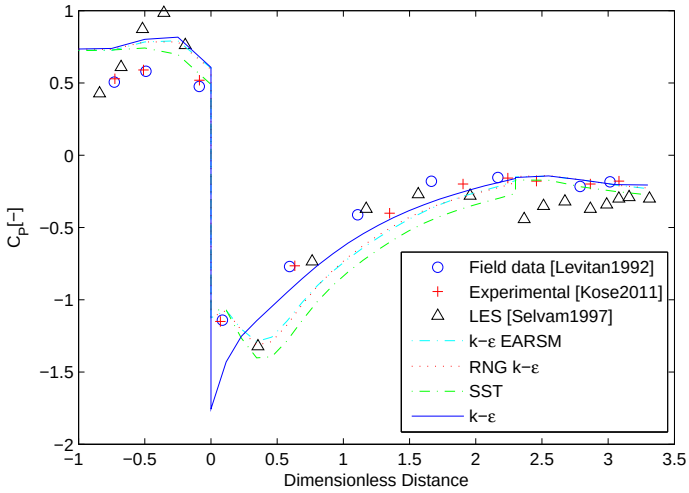

Figure 2.7: Mean pressure coefficient at the centre line of TTU building (parallel to 9.1m wall) with different RANS turbulent models

Pressure coefficient is over estimated on the windward face by all the turbulence models as shown in Fig.2.7 where SST model predicts better than the other two. RNG $k-\epsilon$ and $k-\epsilon$ EARSM predict the roof top pressure coefficient better than standard $k-\epsilon$ and SST turbulence with standard $k-\epsilon$ performing the worst as already explained in [17, 84, 86]. On leeward face SST performs best and predicts the pressure coefficient fairly accurately compared with wind tunnel and field data. Rest of the models behave same on the leeward wall i.e. slightly over predicting the pressure coefficients. Overall SST models perform better on windward and leeward wall with slight over estimation on the roof top compared to the rest three turbulence models. Whereas RNG $k-\epsilon$ and $k-\epsilon$ EARSM almost behave similar and are better on the roof top. It is to be noted that computational results of [86] using LES are very close to field data on the roof top whereas there is over estimation of pressure coefficient on windward and leeward walls. Results reported by [83, 85] using $k-\epsilon$ models do not show much deviation on windward face. Refs. [83, 85] did not use consistent boundary conditions as proposed by [8], however [17] did and reported similar over estimation on the windward face by all turbulent models. Another distinguishing fact is that their computations were done using steady state RANS compared to current study where unsteady formulation is used and results are averaged after all the time steps to obtain the mean pressure coefficients. Therefore a steady state solution is also considered using RNG $k-\epsilon$ turbulence model (SS RNG $k-\epsilon$) and results are shown in Fig.2.8 along with the previous results. Steady state solutions with others are also done but not included as they do not show any improvement. It can be seen that steady state solution predicts the wind loading on the windward side superior than unsteady cases. Also it does not show small pressure reduction on roof corner as exhibited by all current unsteady computational studies as well as LES by [86].

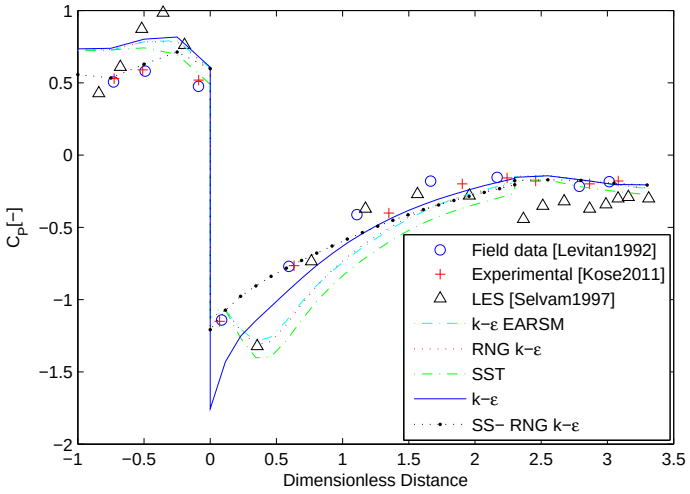

Figure 2.8: Mean pressure coefficient at the centre line of TTU building (parallel to 9.1m wall) with steady and unsteady RANS

Mean horizontal velocity ($\frac{u}{U_{ref}}$) contours are shown in Fig. 2.9 where standard $k-\epsilon$ and RNG $k-\epsilon$ don't capture the roof top vortex, although RNG $k-\epsilon$ shows a small circulation field. Whereas SST model resolves windward roof corner vortex successfully. To resolve such turbulent scales with $k-\epsilon$ models will require a dense mesh because over prediction of turbulent energy and hence eddy viscosity encourages the mixing of turbulent scales near the corner and flow separation does not occur distinctly. Similar conclusions were presented by [17]. All variants of eddy viscosity turbulence models used in current study except standard $k-\epsilon$, predict the wind loading fairly good on low rise building and therefore can be potential candidates for further investigation in our application. From a designer point of view, since SST is slightly over predicting with the right trend, therefore it offers a conservative design. Furthermore it can capture corner vortices (if any) present in the flow at much less computational cost than other eddy viscosity models, thus we plan to use SST model in further study.

2.4 Summary

Consistent inflow profiles to avoid horizontal homogeneity problem in neutral ABL CFD simulation using eddy viscosity turbulence models are presented. A validation study on an experimental low rise building of TTU is also done. It is shown that with a set of boundary conditions deduced from literature review, an accurate neutral ABL can be simulated. Unsteady RANS simulations were performed ats Re of 3×10^6 based on the height and mean velocity at building height. Wind loading in the form of mean pressure coefficient (C_P) over centre line of the TTU building is compared with field data, wind tunnel as well as computational study. Three geometrically progressing set of meshes are used to study mesh convergence. Medium and fine mesh do not show difference in results whereas coarse mesh results are little divergent from other two. Steady RANS with SST resulted in better estimations of mean pressure coefficients on windward face than unsteady formulations. In general a good agreement is achieved between wind tunnel, field data and current computations. Above all right settings in CFX

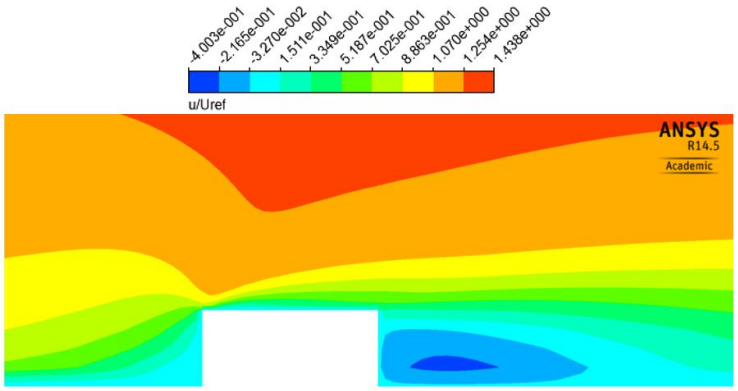

(a) $k - \epsilon$ Model

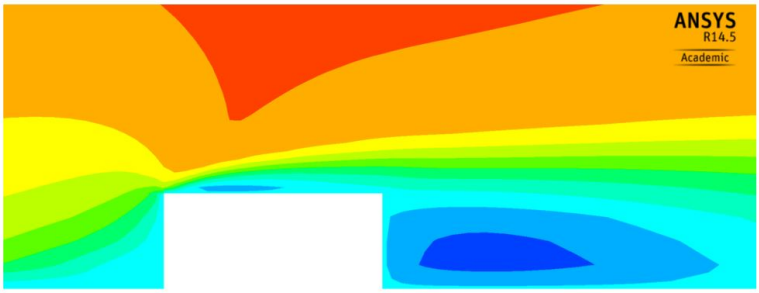

(b) RNG $k - \epsilon$ Model

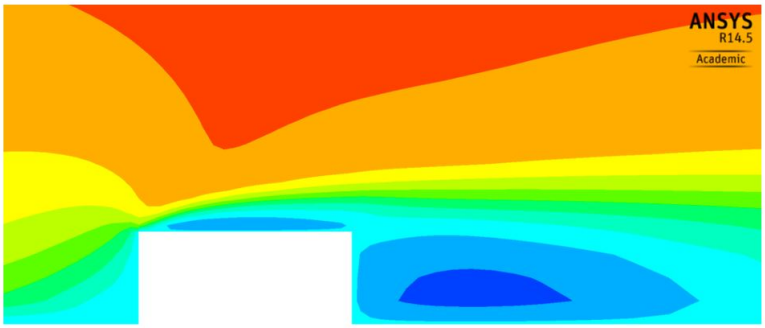

(c) SST Model

Figure 2.9: Dimensionless velocity contours at the center plane of TTU building.

software to simulate neutral ABL are explored that will be further used in next chapter.

3

Wind Loads Estimation on Sunshade using CFD

Contents

3.1 Introduction

CFD can be used successfully to estimate the wind loads on low rise buildings as seen in the previous chapter 2 immersed in turbulent neutral ABL. Furthermore it can also be used to explore the structural response of various structures using Fluid Structure Interaction (FSI). Application of such an analysis has been recently presented by [9] where he analyzed aerodynamic forces and associated non linear structural response of a model tree in ABL. Canopy structures are another example where forces caused by aerodynamic interaction has caused severe damage in Hurricanes Katrina and Rita in US [44]. Open canopy roofs are easy built structures and yet cause severe damage during high speed wind conditions. First documented study for estimating pressure coefficients for structural design of free standing canopy roof was done by Gumley [37]. He performed parametric study to understand effect of roof shape, roof pitch, aspect ratio of roof, eaves height, wind direction and internal stacking arrangement on the generated wind forces [41] using ABL wind tunnel. Same model of was then studied by [38–40] to study mean pressure coefficients and flow physics of leading edge vortex for a flow incident at different angles of attack. While studying wind loading on canopy structure of gasoline station, [44] conducted wind tunnel and CFD studies and concluded that CFD is an adequate tool for finding mean pressures for open structures. ABL CFD simulations have also been applied to understand the wind forces induced on solar modules in free standing and roof mounted configurations [32, 34, 36, 91]. Comparisons of wind tunnel scaled models and CFD full scale computations for wind pressures for a ground mounted solar panel are presented in [31]. Author concludes that CFD studies with correct mean wind profile without even low frequency turbulence are capable of predicting mean wind pressures on the low rise buildings and structures. In this chapter we apply CFD to find pressure loading on our designed sunshade that is subsequently used for structural analysis.

3.2 Numerical Setup

Geometry of the sunshade has been presented in Chapter 1. For current CFD study only top cap is used without any attachments underneath as shown in Fig.3.1. Modeled sunshade is placed in a computational domain of $(20L \times 10L \times 6L)$ where $L = 2.5m$ is the chord length of the sunshade. Domain size and associated boundary condition modeling is shown in Fig. 3.2(a). Guidelines provided by AIJ and COST are considered for domain size selection as discussed in section 2.3.1.A. Consistent set of boundary conditions for correctly simulating ABL deduced from [8, 15] and implemented in chapter 2 are used for this analysis as well. To revisit boundary conditions reader is referred to section 2.3.1.A.

Flow field in the current problem is essentially governed by incompressible Navier-Stokes equations given by eqs. 2.8 and 2.9. As there is no on site mean wind speed measurements available, we use a mean wind speed of $20\frac{m}{s}$ at the height of the sunshade $L = 2.5m$ above the ground. The selected mean wind speed corresponds to *strong gale* where some branches of trees might break off trees and construction signs blow over. On a modern Beaufort scale, it represents wind scale of 9. Such a high speed is selected in order to estimate the wind loads that will be representative of storm loading in

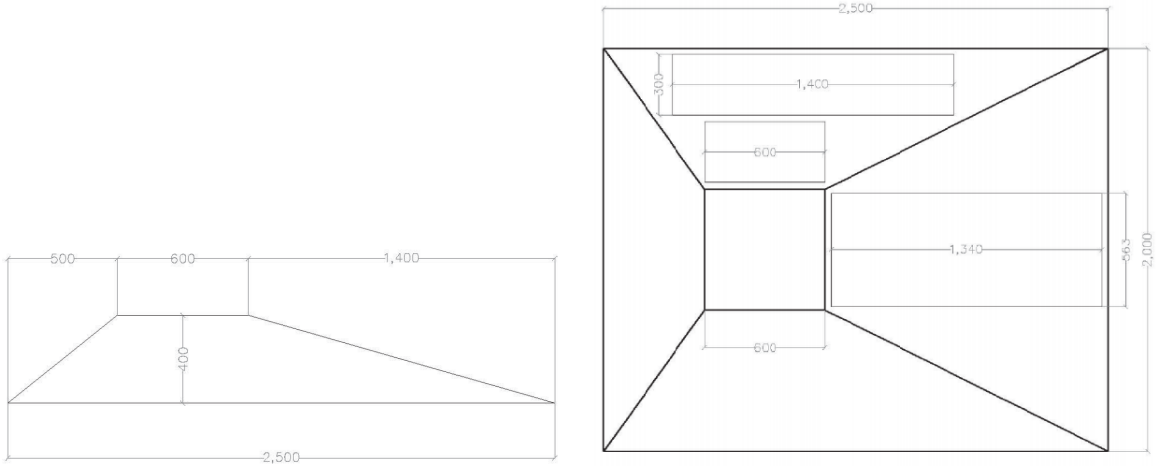

(a) Side view

(b) Top view

(c) Artist rendered view

Figure 3.1: Geometry of the sunshade used for CFD analysis, dimensions are in mm

real scenario. Thus based on the chord length (L), Reynolds number ($Re_L = \frac{U_{ref}L}{\nu}$) of 3×10^6 is simulated. Governing equations are non dimensionalized using mean wind velocity (U_{ref}) as velocity scale and chord length of sunshade (L) as length scale. Turbulence intensity and representative terrain roughness is also assumed to be the same as of validation study measured in field data [82] of TTU building. These conditions generate slightly less than 16% turbulent intensity at the height of the sunshade which is commonly reported turbulence level in open terrain studies using empirical power law as used in [34, 36]. For current study this small difference is ignored.

Domain and sunshade are meshed using a similar strategy as before to have more cells near the point of interest (sunshade) and coarse towards far field. Discritized computational domain is shown Fig. 3.2 where an unstructured mesh using tetrahedral elements is used in the vicinity of sunshade with dense mesh near the edges and relatively coarse over the roof surface as shown in Fig.3.2(c). Number of elements are systematically increased in mesh convergence study using the similar mesh strategy to check the results dependency on mesh.

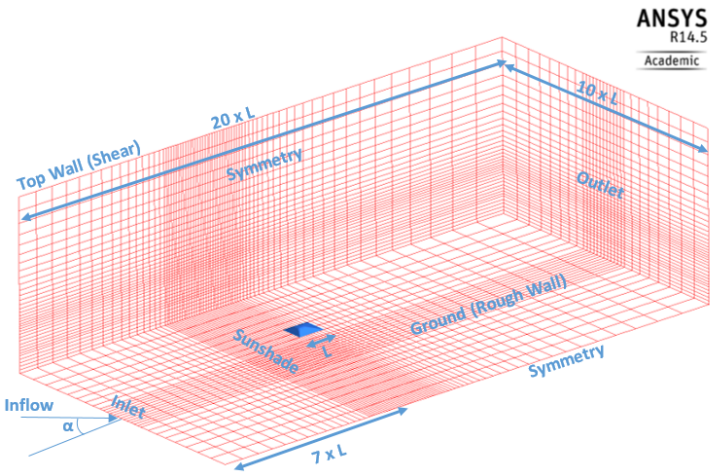

(a) Domain size and boundary conditions

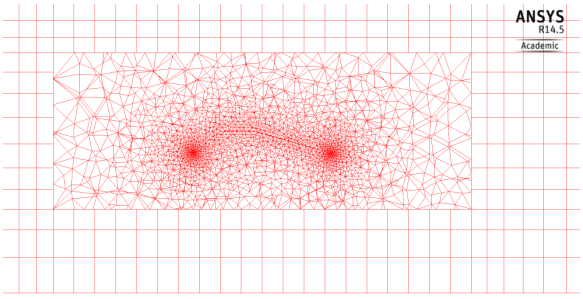

(b) Zoomed view for mesh around sunshade on the center plane of domain

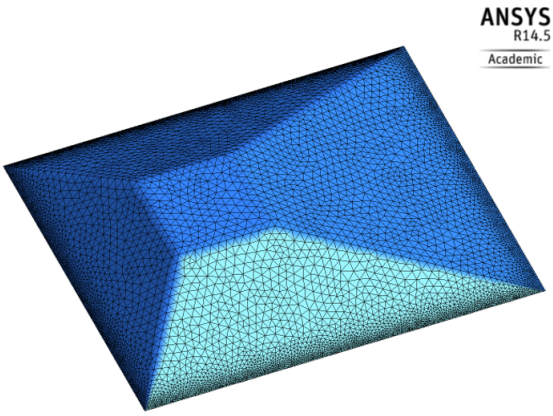

(c) Sunshade surface mesh

Figure 3.2: Computational mesh details of CFD model

3.3 Results and Discussion

A systematic approach to begin with results is taken and explained in this section. Steady state RANS simulation is performed using SST turbulence model for all the cases unless otherwise mentioned specifically. Monitor points near the sunshade are placed to observe velocity, pressure, turbulent kinetic energy and eddy dissipation rate during iterative solutions. A stringent convergence criteria where all r.m.s. residuals are below 1×10^{-8} is set for solution stoppage. Convergence is also considered to be achieved if there is no evident change in variables at the monitor points and all r.m.s. residuals are below at least 1×10^{-6} as outlined in [92]. An example is shown in Fig.3.3 where it can be seen that all results at monitor points defined on the top and below surface of sunshade have achieved steady state solution. A zero degree (flow parallel to chord length of sunshade) of wind incidence angle (α) is simulated in all the cases except the angle of attack study where it is varied to find out the extreme loading scenario.

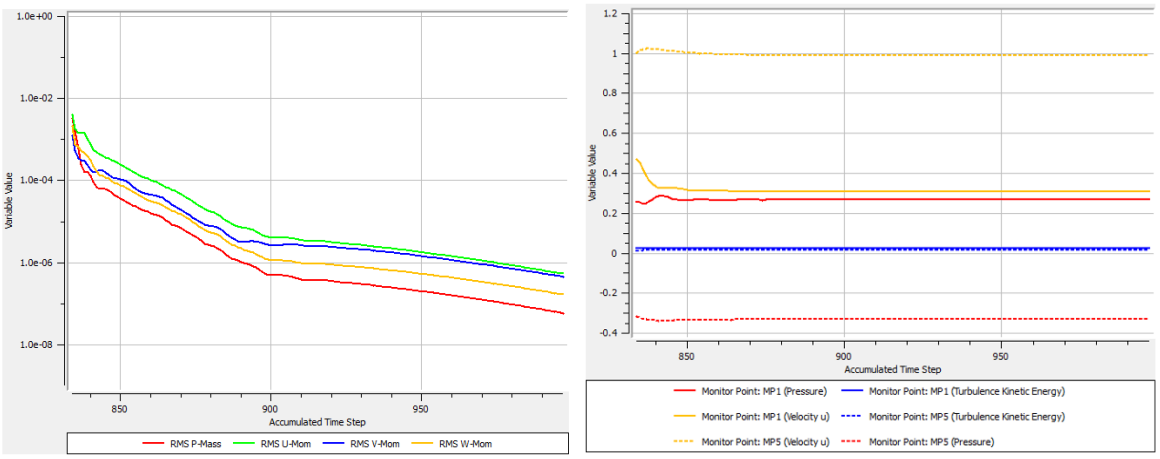

(a) R.m.s residuals

(b) Monitor points

Figure 3.3: An example for solution convergence history

3.3.1 Selection of Sunshade Thickness

CFX is a $3D$ solver and therefore sunshade modeled according to dimensions shown in Fig.3.1 should be given a thickness in order to satisfy the run requirements. Thickness of the sunshade is still an unknown parameter at this stage of design, therefore three small values of non dimensional thickness ($\frac{th}{L}$) 0.001, 0.002 and 0.005 are selected to see the effect of thickness on the results. Attention to the specific turbulence model has not been paid in this section as objective is to find appropriate thickness for solution that will be carried out further and not the actual loading. Pressure coefficient on upper and lower surfaces of the center plane over sunshade, calculated using eq. 2.13 is compared for all three cases in Fig. 3.4. Results on the upper surface are not affected with thickness while on lower surface, results from 0.001 thickness are divergent from others while thickness of 0.002 and 0.005 are the same. Mesh creation using 0.001 thickness causes distorted elements as well which is not observed in other two cases. Furthermore results on the lower surface from 0.001 thickness are less conservative than other two, therefore we select non dimensional thickness of 0.002 for any further analysis.

3.3.2 Neutral ABL Validation

As discussed earlier, validation of neutral ABL is vital for CFD analysis [3, 28, 77]. An empty computational domain is meshed without sunshade inside and boundary conditions from the previous section are implemented in ANSYS CFX. For advection term discritization, default high resolution scheme available in ANSYS CFX is used. As a result of validation study, turbulence is modeled using SST model in this study. Fully developed inflow profiles of mean velocity and turbulence given by eqs. 2.4-2.7 are utilized. Results validate a neutral ABL where inflow profiles do not show significant streamwise gradients as shown in Fig.3.5. Note that turbulence level is slightly less than 15% at the height of the sunshade.

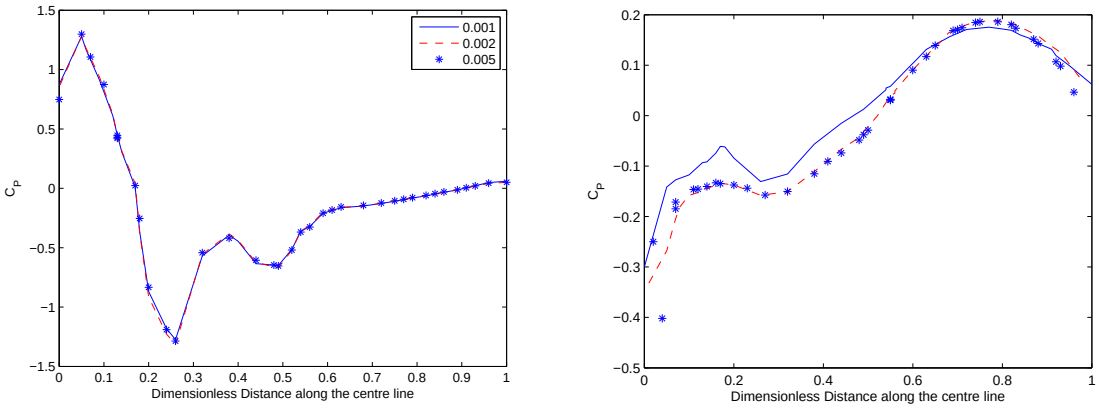

(a) Upper surface **(b)** Lower surface

Figure 3.4: Comparison of mean C_P for different values of sunshade thickness.

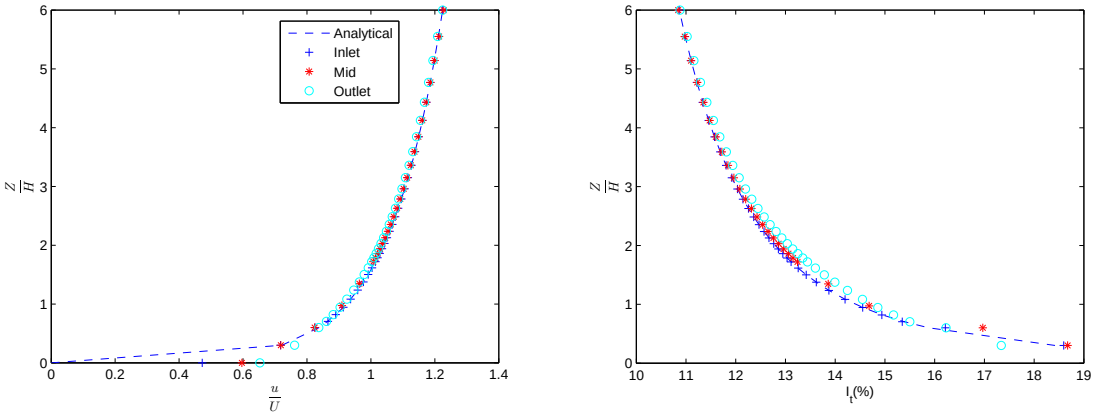

(a) Velocity profile **(b)** Turbulence profile

Figure 3.5: Validation of boundary conditions for horizontal homogeneous ABL.

3.3.3 Mesh Convergence Study

Three sets of mesh namely CaseA, CaseB and CaseC are generated where number of elements are increased in each case for studying mesh convergence study. Geometric progression of 1.1 is used in all cases which is less than maximum of 1.3 recommended by [77]. Details of mesh cases is shown in Table 3.1. Increase in number of elements in CaseB and CaseC is 2.27 and 2.77 times compared to CaseA which is less than recommended value of 3.4 recommended by COST [27]. Note that in current study ANSYS Academic version is used which has limitation of 512 thousand nodes and satisfying requirement of COST would require more nodes than allowed by program, therefore a relatively small fine to coarse ratio is used.

Results on the upper and lower surface at the centre line of sunshade for all three cases are shown in Fig.3.7. Mean pressure coefficient (C_P) on the lower surface is same for CaseB and CaseC setups while suction on windward side of sunshade is overestimated in CaseA. However on the upper surface

Table 3.1: Mesh convergence study for sunshade

Mesh	Elements	Nodes	Size
CaseA	891964	227412	$(27 \times 34 \times 59)$
CaseB	2025322	423093	$(35 \times 43 \times 74)$
CaseC	2473213	499689	$(43 \times 52 \times 92)$

except for the windward corner where CaseC shows the most suction, results from all three cases are practically identical. As explained earlier, finer mesh than this is not possible using academic version of CFX, therefore Case B where results do not vary significantly from CaseC, as a compromise on computational time and accuracy is chosen for next sections.

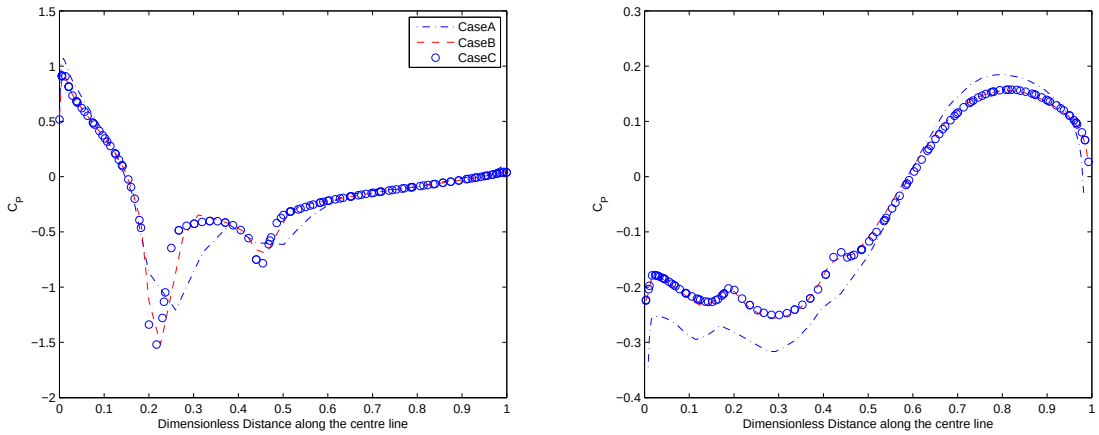

(a) Upper surface **(b)** Lower surface

Figure 3.6: Comparison of mean C_P for different mesh setups.

3.3.4 Comparison of Steady State and Unsteady RANS

Turbulence is a 3 dimensional transient phenomenon and therefore to resolve major scales, time dependent solution of Navier Stokes equations is sometimes necessary. In high rise buildings and bluff bodies immersed in a uniform flow there is von Karman vortex street in wake that requires unsteady formulation of RANS modeling (see for example [93]). However in low rise structures flow is steady in statistical terms and hence most engineering application utilize steady state RANS formulation [94]. To compare the results of both formulation in our case we use unsteady RANS with SST turbulence model. For discretization of convection term in Navier Stokes equation we use high turbulence scheme available in ANSYS CFX whereas second order backward Euler scheme is used for temporal discretization. Simulation is run for a non dimensional time ($t^* = \frac{tU_{ref}}{L}$) of 15 with non dimensional time step of 0.025. Convergence criteria for each outer loop iteration is set as 1×10^{-4} for all r.m.s. residuals. Results are averaged after initial 20 timesteps. For steady state analysis convergence is considered to be achieved when all the residuals stopped changing and this happens when all the residuals are below 1×10^{-6}.

Results from upper surface are equivalent in both cases however transient case results more suction

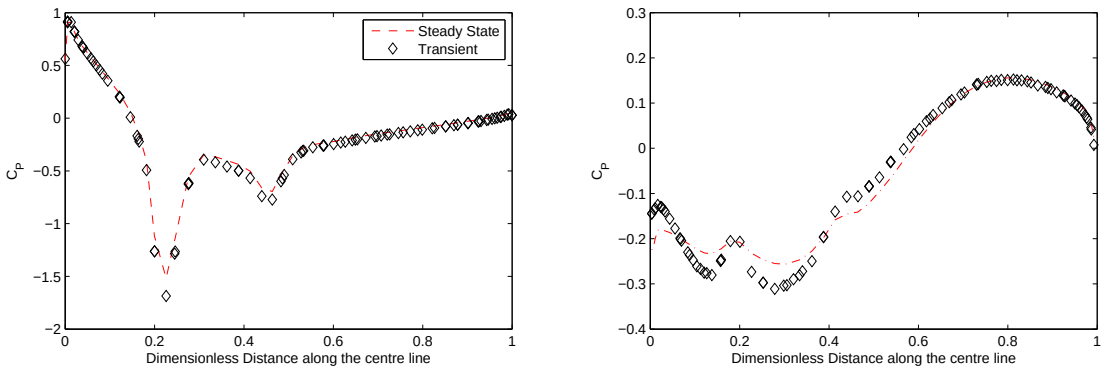

(a) Upper surface **(b)** Lower surface

Figure 3.7: Comparison of steady and unsteady solutions.

towards the windward edge of sunshade on the lower surface compared to steady state solution. Resulting net mean pressure coefficient on the sunshade should be given by eq. 3.1 where $C_{P,U}$ and $C_{P,L}$ represent mean pressure coefficient on upper and lower surfaces respectively [44]. This indicates that resulting pressure loading from steady state analysis will result in conservative case compared to unsteady one. Unsteady solution requires approximately 7.5 hours compared to 1.4 hours in steady state. Furthermore to process the results of all the timesteps for averaging pressure coefficients, unsteady case required 68 GB of memory space which is not feasible for parametric study. Moreover main objective of current work is to estimate pressure loads and not the detailed flow field and since steady state is computationally inexpensive as well as offers conservative design, we choose steady state formulation of RANS for studying effect of different angles of attack on mean pressure coefficient.

$$C_N = C_{P,U} - C_{P,L} \tag{3.1}$$

3.3.5 Effect of Wind Incidence Angle

Wind tunnel testing of open canopy structure of gasoline station studied by [44] showed that extreme wind loading occurs at 30^o angle of attack. Earlier studies of open canopy structures [37, 39] also concluded that 0^o and 30^o are the worst case scenarios. Therefore it is essential to investigate effect of wind incidence angle or angle of attack (α) on pressure loading over sunshade. Angle of attack is varied from 0^o to 240^o with increment of 30^o. In each case all the mesh is kept constant as the CaseB discussed earlier and central block meshed with unstructured tetrahedrons is rotated according to incidence angle. Such an unstructured mesh discritization allowed to change the angle of attack without changing the mesh of whole computational domain saving considerable amounts of time required for remeshing. Steady state cases with solver settings as discussed earlier are used for this study as well. However due to fast solution and easy convergence offered by standard $k-\epsilon$ model, it is used in this investigation. It has been established from validation study and by [27–29, 77, 92] that standard $k-\epsilon$ model over estimates the pressure coefficients on the windward side but it essentially

behaves in the same way as other eddy viscosity models. Therefore in order to have an idea for the worst case scenario, it can be utilized without any problem in present section. Finalized loading to be used for structural analysis will therefore be found out using a case with worst case scenario and SST turbulence model separately. As the mesh points over the surface of sunshade are not same in case of different angle of attack scenarios, therefore in order to compare the results, it is assumed that all data points on the center line are equidistant. This allowed an easy comparison of net mean pressure coefficient (C_N) for various cases along with real distribution on the upper and lower surfaces. Please note that this does not result in actual variation of mean pressure coefficient over center line length (equidistant assumption) rather it makes comparison easy to investigate the extreme loading scenario.

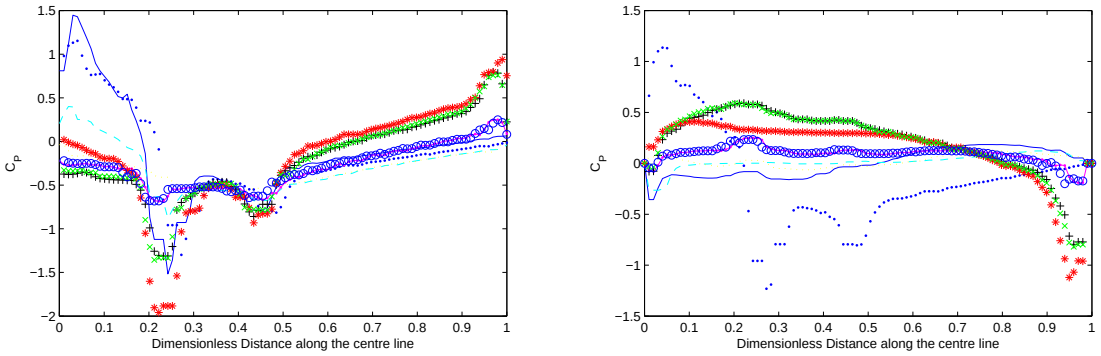

(a) Upper surface **(b)** Lower surface

Figure 3.8: Mean pressure coefficient C_P for various angle of attacks.

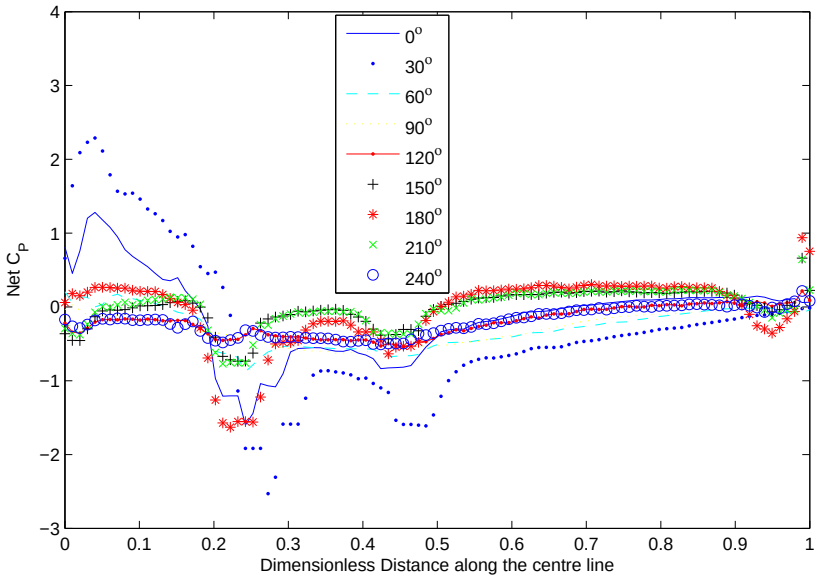

Figure 3.9: Mean net pressure coefficient C_N for various angle of attacks.

Results of the comparative study in the form of mean pressure coefficient C_P on upper and lower

surfaces are shown in Fig. 3.8 and net mean pressure coefficient C_N in Fig. 3.9. Net mean pressure coefficient is calculated using eq. 3.1. The worst loading scenario is simulated with a wind incidence angle (α) of 30^o where windward edge of sunshade experiences positive upwards pressure forces and leeward is under negative pressure loads. These results are in agreement with [37, 44] where maximum loadings are experienced at 30^o angle of attack for a free standing canopy roof. This is then followed by 0^o angle of attack which is also significantly higher than rest of the cases, however lower than 30^o angle of attack. As before, windward face is under upward pressure loading and leeward side including top is experiencing suction. Results show that leeward side of sunshade is under net upwards loading in case of 130^o, 150^o, 180^o and 210^o where magnitude of these loadings is not significant as well, however it again shows negative pressure (suction) near trailing edge. From the results presented it can be concluded that a sunshade designed to withstand loading of 30^o wind incidence angle will survive the wind loadings caused by other wind directions.

3.4 Full Scale Study

In order to get the pressure caused from wind loading, we perform a steady state analysis of full scale model at 0^owind incidence angle and compare the results with non dimensional case dealt earlier. After validation of 0^o case, wind direction of 30^o causing worst loading scenario as seen in previous section is also simulated on full scale to extract pressure loading for subsequent structural analysis. SST turbulence model is used for both cases in order to be consistent with previously investigated scenarios. Geometry and domain are modeled at $1:1$ scale with sunshade thickness of $5mm$ corresponding to non dimensional thickness of 0.002 analyzed earlier. Values of boundary conditions are altered, however profiles still remain the same given by eq.2.4 to 2.7. Surface roughness of the terrain (z_o) is given the value of $17mm$ as provided by [82]. All these boundary conditions resulted in a homogeneous ABL profile validated in empty computational domain as shown in Fig.3.10.

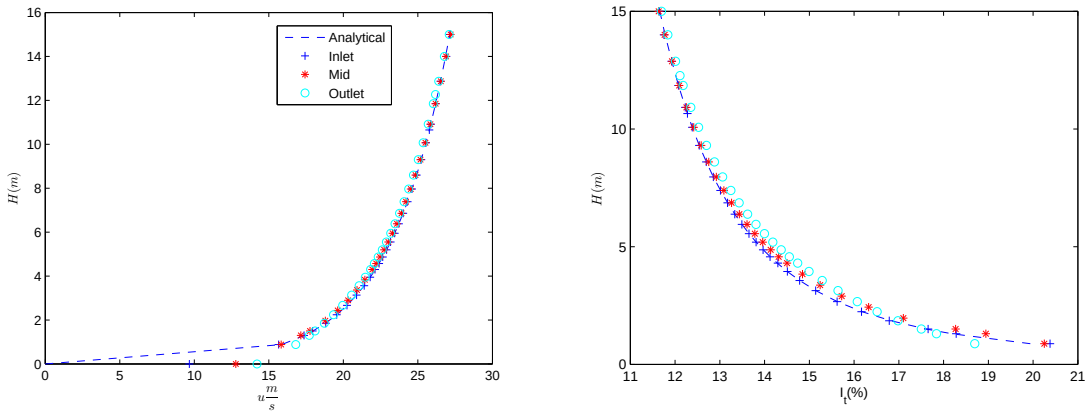

(a) Velocity profile

(b) Turbulence profile

Figure 3.10: Validation of boundary conditions for horizontal homogeneous ABL in case of 1:1 model.

Comparison of non dimensional and full scale models for 0^o wind incidence is shown in Fig.3.11 and

shows a reasonable agreement between two. Small discrepancies can be associated with discritization errors and model constants difference between two scales. For our analysis purposes, we ignore these differences.

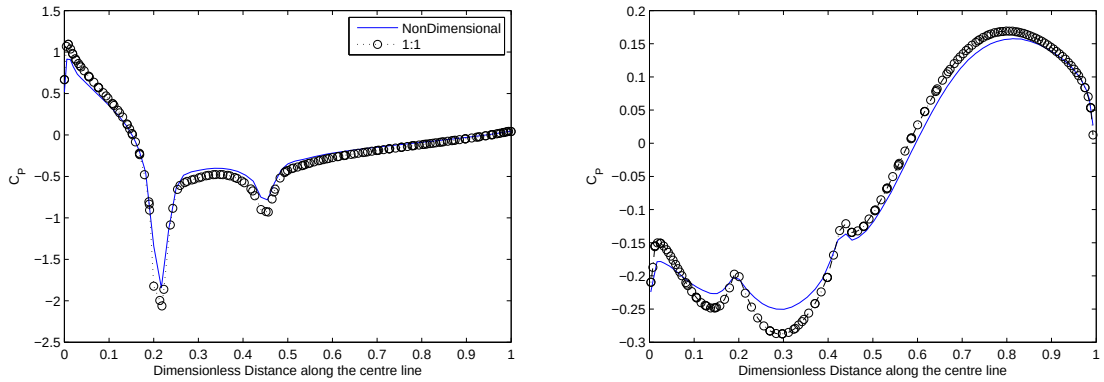

(a) Upper surface **(b)** Lower surface

Figure 3.11: Wind loading comparison between non dimensionalized and 1:1 models.

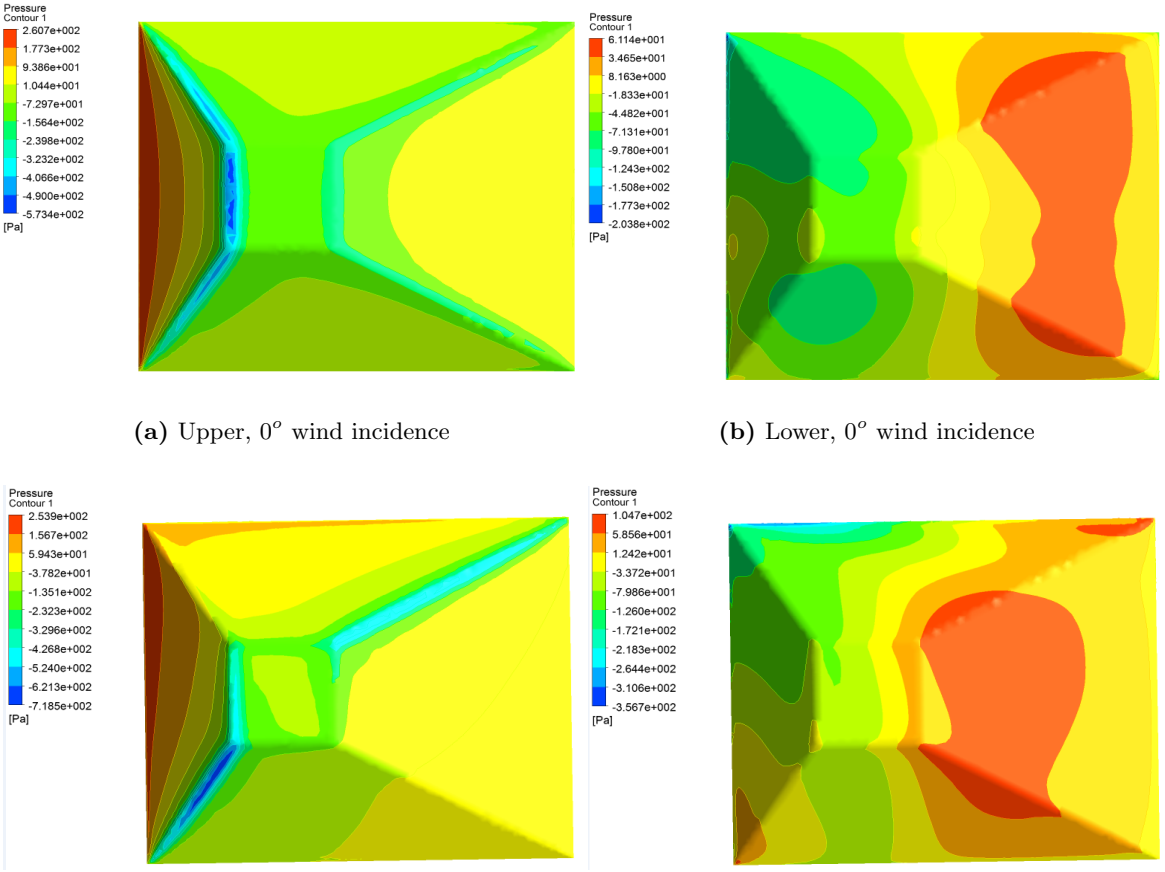

(a) Upper, 0^o wind incidence **(b)** Lower, 0^o wind incidence

(c) Upper, 30^o wind incidence **(d)** Lower, 30^o wind incidence

Figure 3.12: Pressure on the upper and lower surfaces of sunshade for two wind incidence angles.

Results for pressure contours on upper and lower surfaces of sunshade in both wind directions are

shown in Fig.3.12. It can be understood that flow is impinging on the windward side causing maximum pressures of 253.9Pa and 260.682Pa for 0^o and 30^o wind directions respectively. On a general overview it is seen that pressures on the upper surface are extreme in case of 30^o wind incidence angle where maximum suction of -718Pa is observed compared to -573Pa in case of 0^o case. Similar is the case with lower surface where maximum suction pressure of -356.6Pa occurs in case of 30^o compared to -203.76Pa in 0^o wind direction. Pressure loading symmetry is observed in case of parallel flow as shown in Fig.3.12(a) which was anticipated. In case of 30^o wind direction, corners parallel to incoming flow are under less suction forces compared to the others where extreme suctions are observed for the case (Fig.3.12(c)). Overall loadings on both upper and lower surfaces are higher in 30^o case that has already been seen from previous section.

3.5 Pressure Loads Calculation

An ideal scenario for analyzing response of a structure to incoming wind loads is to perform coupled FSI where after every iteration of aerodynamic calculations, loads are transferred to structure causing deformations and then performing aerodynamic analysis further on the deformed structure. However this requires a huge computational expense and is therefore limited to academic research [9]. Also coupled FSI would be necessary for flexible structures which is not the case in current problem. In case of low rise buildings [29] outlines a methodology to transform numerically calculated wind loads in structural design loads by converting it to equivalent static load. However such methodology cant be applied here as the AIJ code mentioned in [29] is focused on buildings. American Society of Civil Engineers (ASCE) [35] also provides guidelines to estimate minimum design loads for structures and in section 6.6, it mentions that wind tunnel modeling can be used to find wind loads on buildings and structures. As CFD study can also reproduce wind tunnel pressure coefficients (upto certain extent), therefore loads from computational studies can also be used for designing wind resisting structures.

A simple approach to extract wind loading from $1:1$ computational studies of 0^o and 30^o is used where we find area averaged pressures P_{av} on upper and lower surfaces of sunshade using eq.3.2. Here P_i, A_i denote elemental pressure and area on a given surface respectively, , N is total elements and A_k is total area of the respective subregion. Upper and lower surfaces are divided into five sub regions as shown in Fig.3.13. Area weighted average is used as advised in ANSYS help [89] because average of nodal values will be biased towards regions of higher mesh density. Similar strategy has been mentioned in Chinese Building code as utilized by [95] for conducting structural analysis of heliostat mounting structure using ABL wind tunnel results.

$$P_{av,k} = \frac{\sum_{i=1}^{N} P_i A_i}{A_k} \tag{3.2}$$

Table 3.2: Pressure (Pa) of sub-regions for 0^o wind incidence angle

Sub region	Upper Surface	Lower Surface	Net
1	70.96	-62.06	133.03
2	-77.01	-26.39	-50.61
3	-59.09	27.28	-86.37
4	-77.49	-30.45	-47.05
5	-170.39	-57.27	-113.13

Table 3.3: Pressure (Pa) of sub-regions for 30^o wind incidence angle

Sub region	Upper Surface	Lower Surface	Net
1	43.86	-65.26	109.12
2	-32.03	-38.47	6.44
3	-79.62	53.57	-133.188
4	-90.74	-2.40	-93.14
5	-181.63	-34.62	-147.02

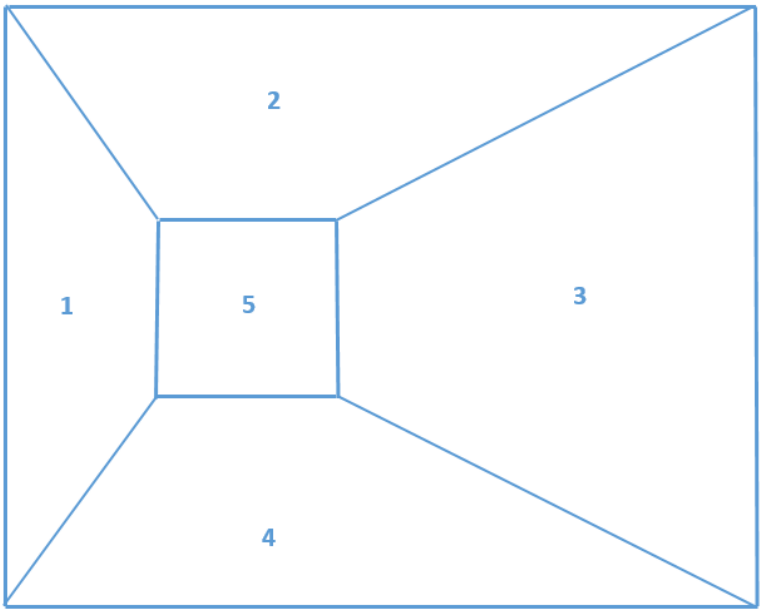

Figure 3.13: Division of upper and lower surfaces into sub regions for average pressure extraction.

Wind incidence angles of 0^o and 30^o realized worst loading scenario as seen in previous section, therefore we present pressures from both cases to be applied on structure. Subregion 1 is under net positive pressure in both cases with maximum loading of 133.03Pa in 0^o angle of attack. Subregions 3, 4 and 5 are experiencing suction forces with maximas in 30^o case. However subregion 2 is under higher suction of -50.61Pa in 0^o case as compared to net upwards pressure of 6.44Pa in 30^o wind direction. In order to design, we will use extreme net pressure values from both cases in the later part of the report.

3.6 Summary

Boundary conditions from validation study are utilized for the current application where flow past designed sunshade is considered. Mesh independence of the solution is shown and comparison of steady state and transient RANS flow analyses with SST turbulence model is presented. It showed that transient loading on the lower surface of the sunshade is deviating from the one estimated using steady state analysis, however due to practicality and computational cost associated with transient simulations, it has not been pursued further. 9 different wind incidence angles are then investigated and qualitative comparison of wind loading on the sunshade in all cases showed that 0^o and 30^o wind directions cause severe loading on the surface of sunshade and encompass all the other cases. To get full scale pressure data, 1:1 model simulations are also performed and results are in reasonable agreement with non dimensional model. Furthermore sunshade is divided into 5 subregions and area weighted averages of pressure are calculated for each sub region. This defines the loading boundary condition for structural analysis in the coming part of the report.

4

Structural Integrity Analysis

Contents

4.1 Introduction

To analyze newly designed structures, numerical techniques are employed instead of costly experimentation. One such numerical tool is FEA where structure is divided into smaller parts called elements and solution for individual elemental nodes is found out. Given that some good practice regulations are followed, FEA can be employed to predict possible behavior of real world structures until failure [5]. In FEA, static structural analysis is usually performed where load variation is considered to be independent of time. On the other hand static response ignores damping and resonance effects are not considered assuming that natural frequency of structure is sufficiently higher than natural frequency of incoming wind flow [49]. Therefore coupled FSI has been preferred in case of thin structures which tend to vibrate and bend with incoming wind, however such investigation comes at much higher computational cost. A recent FSI study for a large thin structure umbrella performed using LES required 90 million node points and simulations took upto 30 days [51]. Static loading available in various standards e.g. [35] generally over estimates the real loading curves. Wind surfer sail under wind loading has been analyzed by [47] and effects of incoming wind on thin roofs were analyzed using static structual anlyses in [45, 46]. Static structural analysis thus can be considered as an appropriate tool defining wind load and required strength of structural members [49].

In this chapter we employ FEA to investigate response of sunshade structure under wind loads evaluated in Chapter3. Two alternative design schemes are explored using static structural analysis. In first scheme we use fiber reinforced composite with plain weave E glass fabric for the top cap of umbrella and second strategy involves conventional Aluminum design. All the modeling and analysis is performed in ANSYS Mechanical APDL software.

4.2 Numerical Setup and Boundary Conditions

Top cap of sunshade is modeled using shell element (Shell181) which is a four node element with six degrees of freedom at each node that is three translational motions and three rotational around x, y and z axes [89]. It can support a lay up scheme required to model composites. We also employ Beam element (Beam188) to model the metallic cross section to be used in the design of top cap of sunshade for case of Aluminum design. Beam188 also has six degrees of freedom at each node and can be assigned any cross sectional area from solid square to a pipe of certain thickness. Dimensions of the geometry according to Fig.3.1 is modeled by drawing keypoints which are further used to make lines that subsequently make areas. Pressure loads are applied on respective areas (Fig.3.13) as per Table3.2 and Table3.3. Worst loading scenario for each patch is selected from 0^o and 30^o wind incidence angle cases. To capture the non linearity in numerical setup, large deformation is turned on in ANSYS as followed by [46, 47, 49]. Application of the load is divided in ten sub steps and maximum of 500 steps are allowed for numerical convergence. In case solution is not converged during these iterations, it stops and problem is investigated for failure. It has been assumed that connection of solar panel on the top and sunshade cap will be done using small bolts and therefore areas Area5 and Area6 in Fig.4.1(a) are constrained in all degrees of freedom i.e. no translational as well as rotational motion is

Table 4.1: Material properties of used composite [4]

E_x (GPa)	E_y (GPa)	E_z (GPa)	G_{xy} (GPa)	G_{yz} (GPa)	G_{zx} (GPa)	ϑ_{xy}	ϑ_{yz}	ϑ_{zx}
26.66	21.07	10.75	5.17	5.05	5.04	0.13	0.34	0.13

allowed at these nodes.

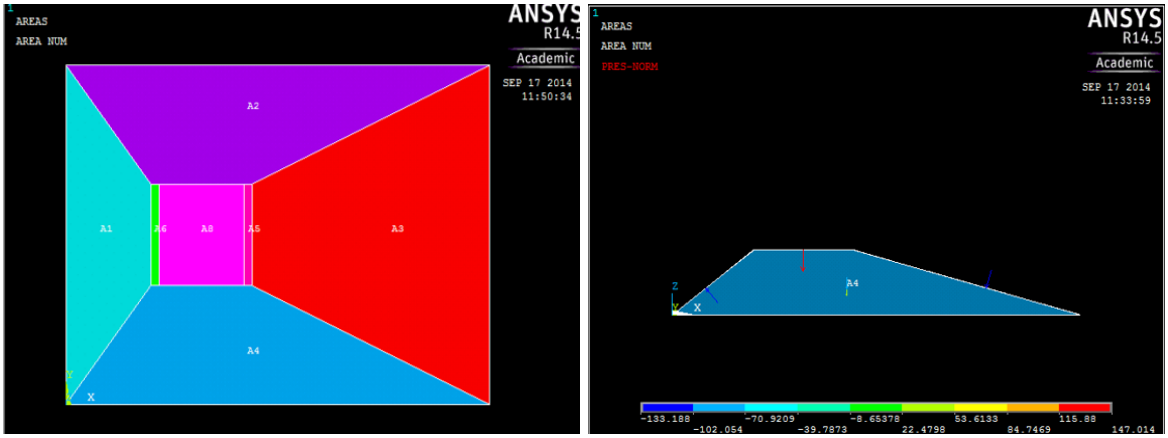

(a) Modeled geometry and area distribution **(b)** Pressure load application

Figure 4.1: Geometry and boundary conditions

4.3 Glass Fiber Composite Case

Due to good corrosion resistant properties and specific mechanical properties, fiber reinforced composite has been used increasingly in recent years by industry [96]. Numerous studies in replacing conventional metallic structural components in automotive as well as aerospace industry are reviewed in [5]. The most common industrial used composite is made from E glass fabric reinforced polymer laminates becuase of its easy manufacturability and less comparative price compared to Kevlar or other carbon reinforced composites. In the current study we use plain weave fiber glass fabric reinforced with vinyl ester resin. Material properties for the composites are strongly dependent on the fiber to resin ratio and varies from one sample to another. In case of orthotropic materials like composite, 9 engineering constants are used to define material completely which are presented in Table4.1 derived from [4]. The ultimate strength of the material in tensile (σ_t) and compressive (σ_c) direction is 280MPa and 180MPa respectively [97]. Similar properties are also mentioned in [98]. Density (ρ_{comp}) of the cured composite part is taken as $1.6\frac{g}{cm^3}$.

4.4 Metallic Case

Conventional design of sunshade employs metallic structure and is therefore explored to compare the outcome of composite studies. Aluminum metal due to its high strength and recycle-ability at the end of life cycle is considered in current application. Aluminum frame is modeled using beam elements

Table 4.2: Material properties of Aluminum

E (GPa)	ϑ
73	0.33

Table 4.3: Cross sectional details of load carrying members

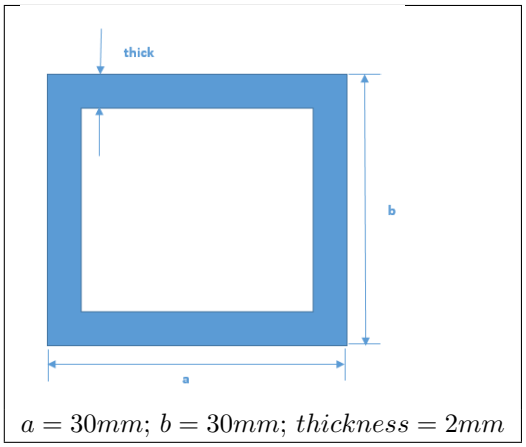

as explained earlier in ANSYS and shown in Fig.4.2. A cross section of hollow square aluminum pipes is used from catalogue of supplier (Alumil Aluminum [99]) with various dimensions of thickness until a reasonable solution is achieved. As in previous case a log file is maintained which allows to change dimensions of selected profile and other solution procedures for iterative study. Material properties and final cross section chosen for the study are summarized in Table4.2 and Table4.3.

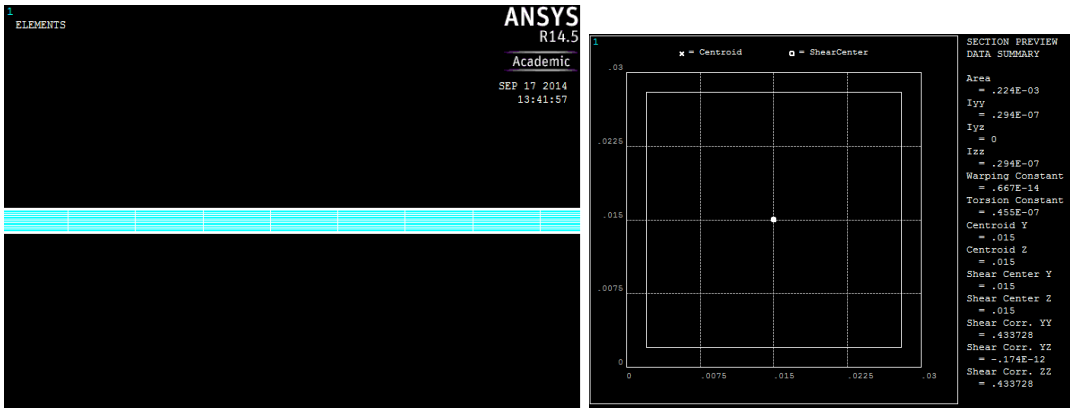

(a) Load carrying member with beam element **(b)** Modeled cross section in ANYS

Figure 4.2: Modeling of structural members in ASNYS using beam element

To distribute the applied pressure load on the load carrying beam members, a thin metallic skin of $1mm$ thickness is modeled and is coupled with the nodes of load carrying members so that there is no independent movement between beams and top skin. Applied boundary conditions are shown in Fig.4.3 where pressure loading is not shown, however it is applied in the same manner as shown in Fig.4.1(b).

Table 4.4: Mesh independence results

Result	CaseA	CaseB	Change (%)	CaseC	Change (%)
Max. Deflection (mm)	26.57	26.21	-1.35	26.10	-0.42
$\sigma_{x,max}$(MPa) First layer	3.5	3.71	6	3.75	1.07
$\sigma_{y,max}$(MPa) First layer	5.05	6.78	34.25	6.27	-7.52
$\sigma_{x,max}$(MPa) Last layer	4.12	4.37	6.06	4.43	1.37
$\sigma_{y,max}$(MPa) Last layer	1.81	2.57	41.9	2.4	-4.28
No. of Elemnts	1125	5100	353.35	14500	184.32

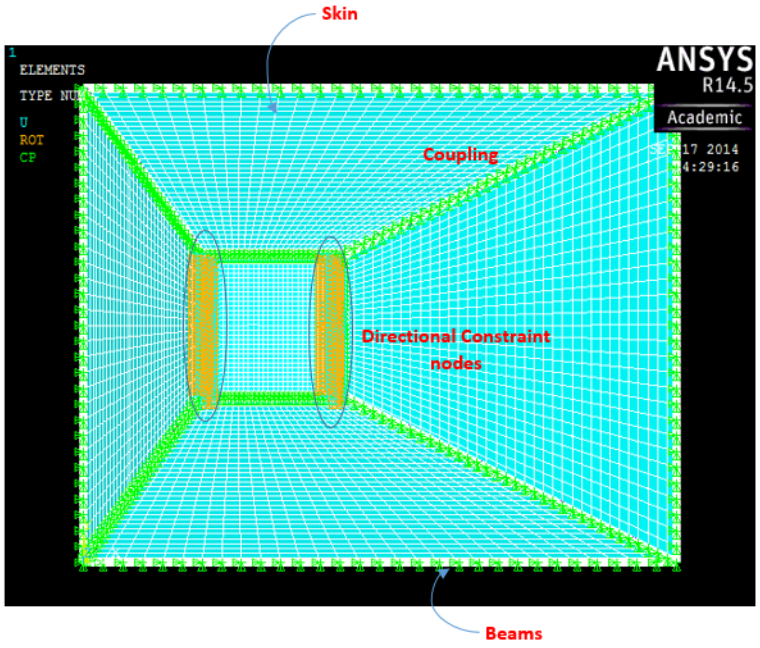

Figure 4.3: Deformation and coupling constraints applied to the FE model

4.5 Results and Discussion

To verify the mesh independence of results, three cases CaseA, CaseB and CaseC are studied. For comparison composite case is considered. Increase in the number of elements from CaseA to CaseB and from CaseB to CaseC is 4.53 and 2.84 respectively. Maximum deflection and stresses in first and last layer of sunshade are compared for all the cases as shown in Table4.4. It can be seen that maximum deflection does not change much between cases and is $26.1mm$ in most refined case compared to $26.21mm$ in case of medium sized mesh (CaseB). Maximum stresses observed in first and last layer of composite sunshade cap are show that maximum property variation from CaseB to CaseC is 7.52% compared to 41.2% from CaseA to CaseB. Thus we use CaseB for any further results.

Sunshade top skin completely made of composite hand layup of 30 cloth layers is selected to present the results. Evolution of total deflection for top layer (30^{th}) at various load steps is presented in Fig.4.4 where it can be seen that rear tip of the canopy is showing deflection of $26.1mm$ which is quite significant for a structure with chord length of $2.5m$. Stresses developed on the other hand are not significant and are well below ultimate strength of composite laminates. Maximum stress encountered in x direction

(σ_x) between first and last layer can be seen in Fig.4.5 which is only 4.43MPa where limiting strength of fiber glass fabric reinforced composite is 280MPa [97]. Similar behavior is observed in y direction where maximum stress (σ_y) is merely 6.27MPa in the first layer as shown in Fig.4.6.

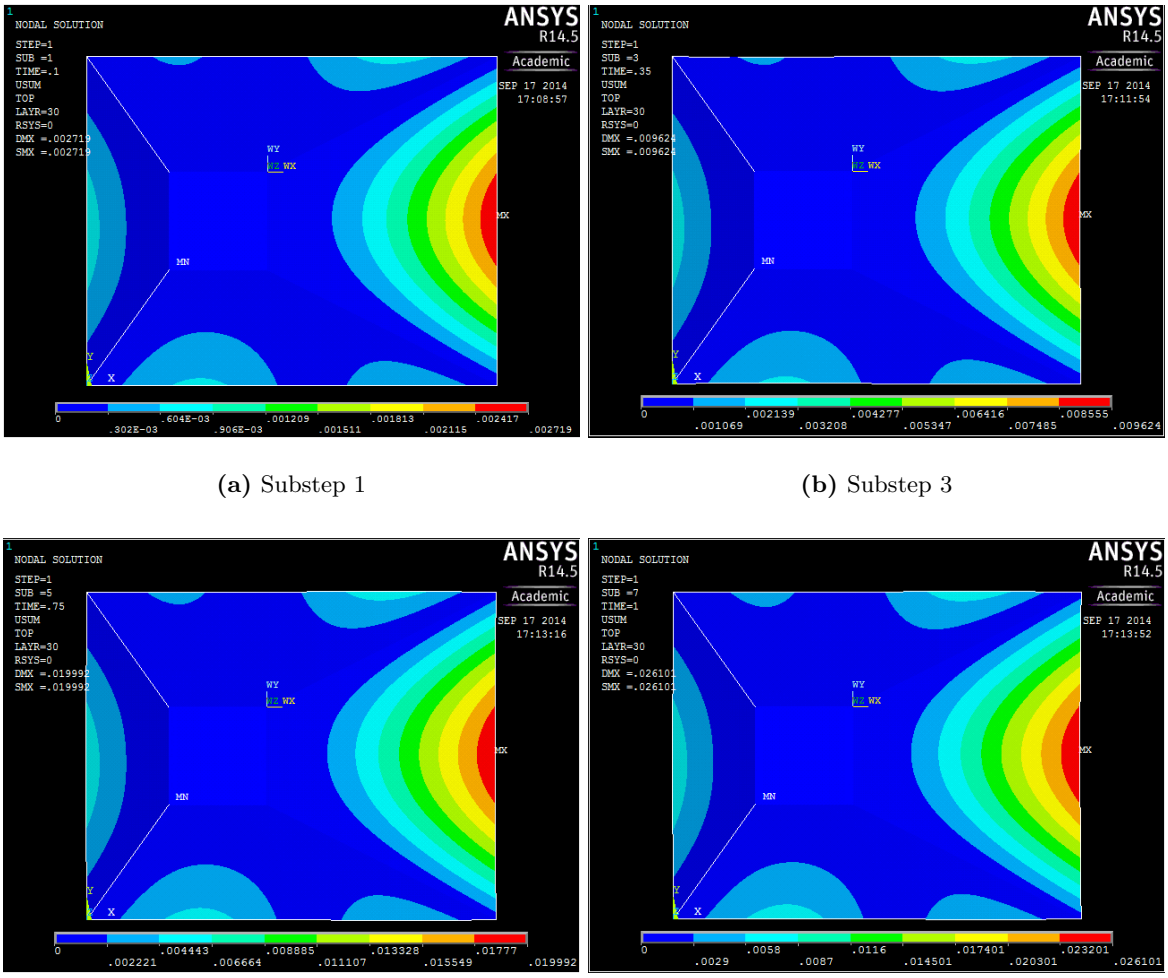

(a) Substep 1

(b) Substep 3

(c) Substep 5

(d) Substep 7

Figure 4.4: Deflection (m) observed during various load steps.

One reason of such low stress levels is high value of deflection for the assembly. As stress signifies the internal resistance of the structure, due to high deflection composite material is not developing significant resistance against applied load. Another reason associated with big deflection is absence of any stiffeners (supporting structure) underneath the composite assembly to hold it. Having metallic inserts during layup process of structural component comes with additional expense, therefore we do not explore scenario of having metallic stiffeners for maintaing shape of sunshade under wind loads.

However scenario where all the structure is considered to be manufactured using standard industrial aluminum prfiled rods is investigated. Deflection at the rear end of the sunshade cap is significantly reduced to 2.4mm compared to 26mm in case of composite material. Whereas von mises stress used to gauge failure of metallic components comes out to be 10.4MPa which is well below the yielding limit of aluminum 20MPa as shown in Fig.4.7. This scenario also provides a safety factor of 1.92.

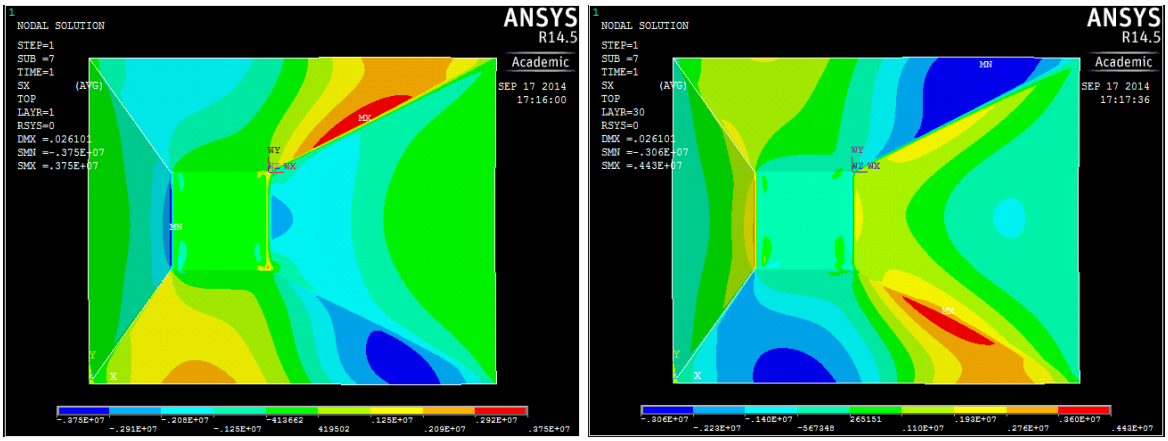

(a) First layer **(b)** Last layer

Figure 4.5: σ_x(MPa) in composite skin.

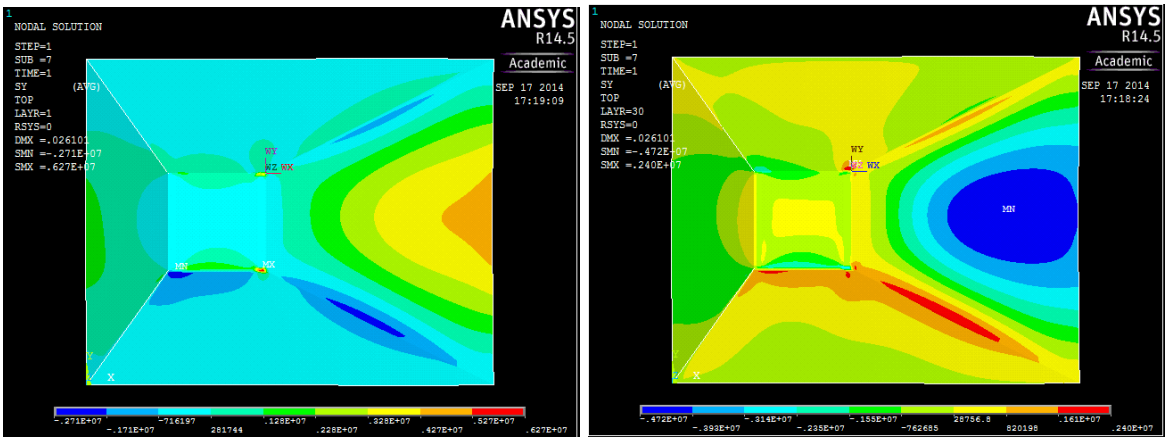

(a) First layer **(b)** Last layer

Figure 4.6: σ_y(MPa) in composite skin.

Comparing weight of the two designs, composite design without stiffeners and 30 layers of fiber glass plain weave fabric results in total mass of 55.78kg calculated using density and volume of modeled layer elements as explained in Appendix. On the other hand standard profiles from Alumil [99] results in total weight of 9.075kg with much less deflection. Composite design is studied for lighter and resilient design of sunshade, however current study shows that weight and overall deflection is not feasible compared to conventional metallic design with aluminum which shows quite practical deflection and stress levels. Maximum deflection is always observed at the rear end of sunshade which poins out that in order to reduce it further, sunshade design might have to be revised and new wind loading dependent on new profile should be calculated which will in turn help to analyze integrity of structure.

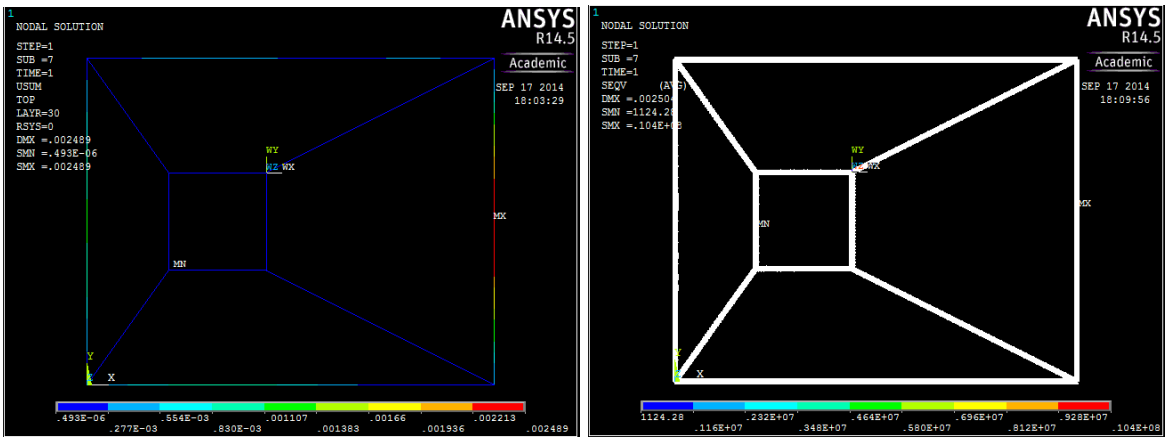

(a) Deflection (m)

(b) von Mises stress

Figure 4.7: Results from metallic design case.

4.6 Summary

Structural analysis using FEA is performed against the calculated wind loads from previous chapter. Two different materials are investigated where one is E glass fiber reinforced composite and other is conventional aluminum metal. Modeling and analysis is done in ANSYS APDL. To iterate efficiently log files for both material designs are written and are attached in Appendix. We have shown that results are independent of mesh refinement. It has been seen that design from composite material shows greatest deflection of 26mm compared to aluminum case. Associated reason for such a big deflection is absence of any stiffeners underneath composite skin, however alternate metallic design shows better results weighing only 9.07kg. Furthermore cosidering the price of raw material and manufacturing, it has been decided to pursue the metallic design further.

5

Summary, Conclusions and Future Work

Contents

5.1 Introduction

The work done in this dissertation is motivated by authors ambition to develop a solar integrated sunshade that can be used to charge hand held devices at resorts and luxury hotels. Market research is carried out during the development of business plan which reveals importance of structural integrity against wind loads for such a structure. Important features of current work are determining wind loads for designed sunshade for wind speed that corresponds to gust using CFD and utilization of resulting loads to analyze the structural strength of design. In this chapter we will present summary of all the work conducted and conclusions drawn out of it. We will also shed some light on the future work that needs to be done in this regard.

5.2 Summary and Conclusions

Numerical methods are employed in engineering applications to reduce the potential failures and even reduce the production times in industry. With the help of such numerical analysis qualitative as well as quantitative features necessary for a design that will meet the end user requirements can be estimated. Physical laws developed by nature can be utilized for benefit of mankind, however they may pose a threat to careless designed structures. One such case is interaction of wind with structures that are immersed in lower part of our atmosphere. Wind exerts pressure force on the structures opposing the flow which has been used to produce clean energy using wind turbines. However collapse of Taconama bridge in 1940 is one such example where wind has excited the structure to the ultimate failure. Thus it necessitates that a designed structure to be used by humans should bear wind loadings without failure. Literature review reveals importance of simulating neutral ABL such that there is no decay in horizontal velocity as well as turbulence characteristics as turbulence dictates the wind suction forces caused to the low rise structures. We have successfully simulated an ABL that is free of any streamwise gradients using CFX. To validate chosen boundary conditions and magnitude of expected pressure forces, we perform flow analysis of a low rise building. TTU building is one of the early research facilities at Texas Technical University for low rise structures. Results of our simulation are compared with field data, wind tunnel as well as numerical studies conducted for pressure around such bluff body immmersed in ABL. A good agreement is observed between current results and previously reported for this low rise building.

We then perform CFD on the potential design of solar sunshade to analyze the pressure forces associated with fluid structure interaction. Velocity corresponding to Beaurofot scale of 9 is selected to perform fluid flow analysis. A relatively high velocity is chosen to simulate the gust like environment in reality. Based on the chord length of the sunshade, we perform CFD analysis at $Re = 3 \times 10^6$. Turbulence is another parameter that dictates magnitude of wind forces by causing shear distribution of the boundary layer. Normal levels of turbulence observed for low rise structures are in order of $15-20\%$ and based upon the validation study and potential application terrain characteristics, we simulate 16% turbulence at the height of the sunshade. Turbulence is modeled using eddy viscosity models or so to speak RANS formulation of Navier-Stokes equations. It has been observed that conventional

$k-\epsilon$ model overestimates the pressure loading on low rise structures by increasing turbulence kinetic energy in the vicinity of structure that may lead to artificial acceleration of fluid. Such artificial accelerations lead to absence of primary rooftop vortex observed in natural flow over bluff bodies. Modified $k-\epsilon$ models resolve this issue and therefore we use shear stress transport (SST) turbulence model to accomodate turbulence in numerical flow study. It has been found out through literature review that to best capture turbulent characteristics of natural flows, LES should be pursued, however due to high computational cost associated with modeling all the big turbulence scales and modeling the small using certain formulations, LES is not usually pursued in industry and therefore computational wind engineering still heavily relies on RANS model.

To estimate the worst loading scenario, 9 different wind directions are investigated with an aim to have qualitative understanding of force magnitude. To compare the results in between different wind incidence angle cases, net mean pressure coefficient (C_N) is calculated using mean pressure coefficients at the upper and lower skins of sunshade. Results show that extreme loading is expected at 30^o and 0^o wind flow directions. Windward side of sunshade experiences net positive upwards forces whereas leeward side is under suction forces. To cater for the dimensional effects, we then perform a $1:1$ scale CFD and to generate the pressure loading that can be readily used for subsequent structural analysis. After that we divide the sunshade in 5 zones where net mean pressure is calculated using area average pressure at each surface. This has led us to define a representative mean pressure to be applied on the individual surfaces for investigating structural response of the structure.

For carrying out the numerical analysis to estimate the structural integrity, we perform FEA where structure is divided into small elements and nodal solution of governing equations is found on the individual elements. Two alternative approach for structural design are considered. Due to high specific strength and insulating properties of composites, fiber reinforced composite with E-glass plain weave fabric for the design of sunshade canopy is studied. Modeling was done using Shell181 element in ANSYS which allows to model lay up procedure as observed in industrial manufacturing of composites. Alternate study with aluminum pipes with hollow square cross section is also investigated where standard industrial aluminum profiles from Alumil [99] is used. Iterative methodology to reach upto reasonable solution is adopted where a programmable input file is written to be input in ANSYS that allows change in number of fabric layers in case of composite design and cross section of aluminum pipes in alternate design. It has been seen that without any internal structure that is stiffeners, composite design with combined thickness of $5.4mm$ undergoes deflection of $26.10mm$ at the leeward end. Whereas design with aluminum pipes with a cross section of $20mm \times 20mm \times 2mm$ results in deflection of only $2.4mm$ which is in practical range with von-Mises stress of 10.4MPa giving a design with safety factor of 1.92. Furthermore resulting weight from aluminum design is 9.07kg compared to 55.78kg in case of composite. Therefore a metallic design promises a lightweight and cheap solution for the sunshade under study and will be followed for manufacturing.

This work has been conducted to lay down a methodology by which engineering disciplines can be applied for the resilient design in the early stages of product development cycle. Preliminary analysis conducted shows that high manufacturing cost and design complexity, composite material can

not be used in our application. In order for composite design to work, internal structure has to be added to resist present significant deflection and this directly contributes to cost, whereas metallic structure made of aluminum is cheaper and provides a cost competitiveness in intended market for such a product. For a product to be qualified for EU green certification which is the ultimate goal of author, conventional industrial composite materials can not be utilized as they do not offer any recycleability at the end of lifecycle and hence contribute towards environmental waste. On the other hand, aluminum is easily recycleable and a structure made out of recycled aluminum certainly qualifies the goals of green design and serves best the ideology of company.

5.3 Future Work

Although RANS is being used heavily in computational wind engineering, it still lacks the important scales of turbulence and hence LES should be pursued further to improve the design. Current work has been done using ANSYS Academic which is a student version of main commercial code and it has certain limitations. During the mesh refinement study of sunshade flow analysis, we could not achieve excellent grid independence due to program limitation of $512k$ nodes. This certainly has to be checked with full version for improved results. In present study wind loading has been characterized by mean pressure coefficients on the surface of sunshade, however in order to obtain peak pressure loadings transient study will be pursued in future that may lead to increased peak pressure loading.

Structural analysis performed misses engineering details of the final assembly. In order to improve results, top of the sunshade should be modeled along with bolts to see the effect of wind loading on the bolts and their yielding if any. Including these small details would not change the design substantially, however it will help deciding required dimensions and number of bolts necessary to hold the structure against incoming wind loads. Furthermore load is distributed using a thin metallic skin in case of aluminum design which does not represent the real case and is an approximation. Future work will be done to incorporate a pre-stressed cloth from manufacturers which however needs experimental testing to determine forces required to model pre-stressing of cloth using FEA.

Bibliography

[1] J. Kaimal and J. Finnigan, *Atmospheric boundary layer flows : their structure and measurement.* Oxford University Press, New York. ISBN-13:978-0195062397, 1994.

[2] "Wikipedia," http://www.wikipedia.org, 2011.

[3] B. Blocken, T. Stathopoulos, and J. Carmeliet, "CFD simulation of the atmospheric boundary layer: wall function problems." *Atmospheric Environment 41(2), 238-252*, 2007.

[4] Y. Shindo, S. Takahashi, T. Takeda, F. Narita, and S. Watanabe, "Mixed-mode interlaminar fracture and damage characterization in woven fabric-reinforced glass/epoxy composite laminates at cryogenic temperatures using the finite element and improved test methods." *Engineering Fracture Mechanics 75, 5101-5112*, 2008.

[5] P. Maropoulos and D. Ceglarek, "Design verification and validation in product life cycle." *CIRP Annals- Manufacturing Technology 59, 740-759*, 2010.

[6] E. Mathews, "Prediction of the wind-generated pressure distribution around building." *Journal of Wind Engineering and Industrial Aerodynamics 25, 219-228*, 1987.

[7] P. Richards and B. Younis, "Comments on "Prediction of the wind-generated pressure distribution around building" by E.H. Mathews." *Journal of Wind Engineering and Industrial Aerodynamics 34, 107-110*, 1990.

[8] P. Richards and R. Hoxey, "Appropriate boundary conditions for computational wind engineering models using k-ϵ turbulence model." *Journal of Wind Engineering and Industrial Aerodynamics 46-47, 145-153*, 1993.

[9] A. Aly, "Atmospheric boundary-layer simulation for the built environment: Past, present and future." *Building and Environment 75, 206-221*, 2014.

[10] C. Zhang, " Numerical prediction of turbulent recirculating flows with a $k-\epsilon$ model." *Journal of Wind Engineering and Industrial Aerodynamics 51, 177-201*, 1994.

[11] M. Tsuchiya, S. Murakami, A. Mochida, K. K., and Y. Ishida, "Development of new $k-\epsilon$ model for flow and pressure fields around bluff body." *Journal of Wind Engineering and Industrial Aerodynamics 67 & 68(3), 169-182*, 1997.

[12] A. Mochida, Y. Tominaga, S. Murakami, R. Yoshie, T. Ishihara, and R. Ooka, "Comparison of various $k-\epsilon$ models and DSM applied to flow around a high-rise building- Report on AIJ cooperative project for CFD prediction of wind environment." *Wind Struct. 5 (2-4), 227-244*, 2002.

[13] J. Walshe, "CFD modeling of wind flow over complex and rough terrain." *PhD Thesis, University of Loughborough*, 2003.

[14] A. Riddle, D. Carruthers, A. Sharpe, C. McHigh, and J. Stocker, "Comparisons betwen Fluent and ADMS for atmospheric dispersion modeling." *Atmospheric Environment 38, 1029-1038*, 2004.

[15] P. Richards and S. Norres, "Appropriate boundary conditions for computational wind engineering models revisited." *Journal of Wind Engineering and Industrial Aerodynamics 99, 257-266*, 2011.

[16] D. Hargreaves and N. Wright, "On the use of k-ϵ model in commercial CFD software to model the neutral atmospheric boundary layer." *Journal of Wind Engineering and Industrial Aerodynamics 95, 355-369*, 2007.

[17] T. Guha, R. Sharma, and P. Richards, "CFD modeling of wind induced mean and fluctuating external pressure coefficients on the Texas Tech University building," *Proceedings of 5th European African conference on wind engineering, Italy*, 2009.

[18] J. Sullivan, R. Archer, and R. Flay, "Consistent boundary conditions for flows with in the atmospheric boundary layer." *Journal of Wind Engineering and Industrial Aerodynamics 99, 65-77*, 2011.

[19] M. Levitan, K. Mehta, and W. Vann, "Field measurements of pressures on the Texas Tech building." *Journal of Wind Engineering and Industrial Aerodynamics 38, 227-234*, 1991.

[20] Y. Yang, M. Gu, S. Chen, and X. Jin, "New inflow boundary conditions for modeling the neutral equilibrium atmospheric boundary layer in computational wind engineering." *Journal of Wind Engineering and Industrial Aerodynamics 97(2), 88-95*, 2011.

[21] G. C., vanBeeck J., R. P., and V. G., "CFD modeling of small particle dispersion: the influence of the turbulent kinetic energy in the atmospheric boundary layer." *Atmospheric Environment 43, 673-681*, 2009.

[22] A. Parente, C. GorleÂ´, van Beeck J., and C. Benocci, "Improved $k-\epsilon$ model and wall function formulation for the RANS simulation of ABL flows." *Journal of Wind Engineering and Industrial Aerodynamics 99, 267-278*, 2011.

[23] D. Kose, D. Fauconnier, and E. Dick, "ILES of flow over low-rise buildings: Influence of inflow conditions on the quality of the mean pressure distribution prediction." *Journal of Wind Engineering and Industrial Aerodynamics 99, 1056-1068*, 2011.

[24] M. Balogh, A. Parente, and C. Benocci, "RANS simulation of ABL flow over complex terrains applying an Enhanced k-emodel and wall function formulation: Implementation and comparison for fluent and OpenFOAM." *Journal of Wind Engineering and Industrial Aerodynamics 104-106, 360-368*, 2012.

[25] F. Juretic and H. Kozmar, "Computational modeling of the neutrally stratified atmospheric boundary layer flow using the standard $k-\epsilon$ turbulence model." *Journal of Wind Engineering and Industrial Aerodynamics 115, 112-120*, 2013.

[26] A. Jakeman, R. Letcher, and J. Norton, "Ten iterative steps in development and evaluation of environmental models." *Environmental Modelling & Software 21 (5), 602-614*, 2012.

[27] J. Franke, "Recommendations of the COST action C14 on the use of CFD in predicting pedestrian wind environment." in *Proceedings of 4th International Symposium on Computational Wind Engineering (CWE2006)*, Yokohama, Japan, 2006.

[28] A. Tominaga, Y.and Mochida, R. Yoshie, H. Kataoka, T. Nozu, M. Yoshikawa, and T. Shirasawa, "AIJ guidelines for practical applications of CFD to pedestrian wind environment around buildings." *Journal of Wind Engineering and Industrial Aerodynamics 96, 1749-1761*, 2008.

[29] T. Tamura, K. Nozawa, and K. Kodno, "AIJ guide for numerical prediction of wind loads on buildings." *Journal of Wind Engineering and Industrial Aerodynamics 96, 1974-1984*, 2008.

[30] B. B., J. W.D., and S. T., "CFD evaluation of wind speed conditions in passages between parallel buildings- effect of wall-function roughness modifications for the atmospheric boundary layer flow." *Environmental Modelling & Software 30, 15-34*, 2012.

[31] A. Aly and G. Bitsuamlak, "Aerodynamics of ground-mounted solar panels: Test model scale effects." *Journal of Wind Engineering and Industrial Aerodynamics 123, 250-260*, 2013.

[32] R. Pratt and G. Kopp, "Velocity measurements around low-profile, tilted, solar arrays mounted on large flat-roofs, for wall normal wind directions." *Journal of Wind Engineering and Industrial Aerodynamics 123, 226-238*, 2013.

[33] T. Stathopoulos, I. Zisis, and E. Xypnitou, "Local and overall wind pressure and force coefficients for solar panels." *Journal of Wind Engineering and Industrial Aerodynamics 125, 195-206*, 2014.

[34] M. Shademan and H. Hangan, "Wind Loading on Solar Panels at Different Inclination Angles." in *Proceedings of 11th Americas Conference on Wind Engineering (CWE2010) San Juan, Puerto Rico*, 2009.

[35] A. S. of Civil Engineers, *Minimum design loads for buildings and other structures, Revision ASCE7-98.* American Society of Civil Engineers, Virginia USA., 2013.

[36] G. Bitsuamlak, A. Dagnew, and J. Erwin, "Evaluation of wind loads on solar panel modules using CFD." in *Proceedings of Fifth International Symposium on Computational Wind Engineering (CWE2010) Chapel Hill, North Carolina, USA*, 2010.

[37] S. Gumley, "A Parametric Study of Extreme Pressures for the Static Design of Canopy Structures." *Journal of Wind Engineering and Industrial Aerodynamics 16, 43-56*, 1984.

[38] J. Ginger and C. Letchford, "Peak wind loads under delta wing vortices on canopy roofs." *Journal of Wind Engineering and Industrial Aerodynamics 41-44, 1739-1750*, 1992.

[39] C. Letchford and J. Ginger, "Wind loads on planar canopy roofs - Part 1: Mean pressure distributions ." *Journal of Wind Engineering and Industrial Aerodynamics 45, 25-45*, 1992.

[40] J. Ginger and C. Letchford, "Wind loads on planar canopy roofs, Part 2: fluctuating pressure distributions and correlations." *Journal of Wind Engineering and Industrial Aerodynamics 51, 353-370*, 1994.

[41] Y. Uematsu and T. Stathopoulos, "Wind loads on free-standing canopy roofs: a review." *Journal of Wind Engineering 95, 245-256*, 2003.

[42] Y. Uematsu, T. Stathopoulos, and E. Iizumi, "Wind loads on free-standing canopy roofs: Part 1 local wind pressures." *Journal of Wind Engineering and Industrial Aerodynamics 96, 1015-1028*, 2008.

[43] ——, "Wind loads on free-standing canopy roofs: Part 2 overall wind forces." *Journal of Wind Engineering and Industrial Aerodynamics 96, 1029-1042*, 2008.

[44] A. Poitevin, B. Natalini, and L. Godoy, "Pressures on open canopy structures with parapets under wind loading." *Engineering Structures 56, 850-867*, 2013.

[45] J. Diaz, P. Neito, and F. Dominguez, "Numerical analysis of pressure field on curved self-weighted metallic roofs due to the wind effect by the finite element method." *Journal of Computational and Applied Mathematics 192, 40-50*, 2006.

[46] J. Diaz, P. Neito, J. Perez, and A. Navarro, "Numerical analysis of the pressure field on curved and open self-weighted metallic roofs due to the wind effect by the finite volume method." *Journal of Applied Mathematics and Computation 209, 31-41*, 2009.

[47] A. Blicblau, M. Singh, E. McConnel, and M. Pleaner, "Stress analysis of a novice windsurfer sail by finite element analysis." *Journal of Mathematical and Computer Modeling 47, 1108-1116*, 2006.

[48] D. Briassoulis and A. Mistriotis, "Integrated structural design methodology for agricultural protecting structures covered with nets." *Biosystems Engineering 105, 205-220*, 2010.

[49] A. Schellenberg, J. Maffei., K. Telleen, and R. Ward, "Structural analysis and application of wind loads to solar arrays." *Journal of Wind Engineering and Industrial Aerodynamics 123, 261-272*, 2013.

[50] A. Michelski, P. Kermel, E. Haug, R. Lohner, R. Wuchner, and K. Bletzinger, "Validation of computational fluid-struture interaction simulation at real scale tests of a flexible 29m umbrealla

in natural wind flow." *Journal of Wind Engineering and Industrial Aerodynamics 99, 400-413*, 2011.

[51] A. Michalski, D. Britto, P. Gellene, and E. Haug, "Computational wind engineering of light weight structures." in *Proceedings of Sixth European and African conference on wind engineering*, Cambridge, UK, 2013.

[52] B. Leitl, P. Kastner-Klein, M. Rau, and R. Meroney, "Concentration and flow distributions in the vincinity of u-shaped buildings: wind-tunnel and computational data." *Journal of Wind Engineering and Industrial Aerodynamics 67-68, 745-755*, 1997.

[53] R. Meroney, B. Leitl, S. Rafailidis, and M. Schatzmann, "Wind-tunnel and numerical modelling of flow and dispersion about several building shapes." *Journal of Wind Engineering and Industrial Aerodynamics 81, 333-345*, 1999.

[54] S. A. Garcia, J. van Beeck, P. Rambaud, and D. Olivari, "Numerical and experimental modelling of pollutant dispersion in a street canyon." *Journal of Wind Engineering and Industrial Aerodynamics 90, 321-339*, 2002.

[55] C. Chang and R. Meroney, "Concentration and flow distributions in urban street canyons: wind tunnel and computational data." *Journal of Wind Engineering and Industrial Aerodynamics 91, 1141-1154*, 2003.

[56] A. Chu, R. Kwok, and K. Yu, "Study of pollution dispersion in urban areas using Computational Fluid Dynamics (CFD) and Geographic Information System (GIS)." *Environmental Modelling & Software 20 (3), 273-277*, 2005.

[57] E. Canepa, "An overview about the study of downwash effects on dispersion of airborne pollutants." *Environmental Modelling & Software 19 (12), 1077-1087*, 2004.

[58] N. Dixon, J. Boddy, R. Smalley, and A. Tomlin, "Evaluation of a turbulent flow and dispersion model in a typical street canyon in York, UK." *Atmospheric Environment 40, 958-972*, 2006.

[59] X. Wang and K. McNamara, "Effects of street orientation on dispersion at or near urban street intersections." *Journal of Wind Engineering and Industrial Aerodynamics 95, 1526-1540*, 2007.

[60] M. Mokhtarzadeh-Dehghan, A. Akcayoglu, and A. Robins, "Numerical study and comparison with experiment of dispersion of a heavier-than-air gas in a simulated neutral atmospheric boundary layer." *Journal of Wind Engineering and Industrial Aerodynamics 110, 10-24*, 2012.

[61] Q. Chen, " Effect of fluctuating wind direction on cross natural ventilation in buildings from large eddy simulation." *Build. Environ. 37 (4), 379-386*, 2002.

[62] ——, "Ventilation performance prediction for buildings: a method overview and recent applications." *Build. Environ. 44 (4), 848-858*, 2009.

[63] B. Blocken and J. Carmeliet, "A review of wind-driven rain research in building science." *Journal of Wind Engineering and Industrial Aerodynamics 92 (13), 1079-1130*, 2004.

[64] S. Huang and Q. Li, "Numerical simulations of wind-driven rain on building envelopes based on Eulerian multiphase model." *Journal of Wind Engineering and Industrial Aerodynamics 98(12), 843-857*, 2010.

[65] B. Blocken and J. Carmeliet, "The influence of wind blocking effect by a building on its wind driven rain exposure." *Journal of Wind Engineering and Industrial Aerodynamics 94(2), 101-127*, 2006.

[66] Y. Tominaga and A. Mochida, "CFD prediction of flow field and snowdrift around a building complex in a snowy region." *Journal of Wind Engineering and Industrial Aerodynamics 81 (1-3), 273-282*, 1999.

[67] A. Hussein and H. El-Shishiny, "Influences of wind flow over heritage sites: a case study of the wind environment over the Giza Plateau in Egypt." *Environmental Modelling & Software 24 (3), 389-410*, 2009.

[68] R. GoÂ´mez-Elvira, A. Crespo, E. Migoya, F. Manuel, and J. HernaÂ´ndez, " Anisotropy of turbulence in wind turbine wakes." *Journal of Wind Engineering and Industrial Aerodynamics 93, 797-814*, 2005.

[69] A. Kasmi and C. Masson, "An extended $k - \epsilon$ model for turbulent flow through horizontal-axis wind turbines." *Journal of Wind Engineering and Industrial Aerodynamics 96, 103-122*, 2008.

[70] S. Milashuk and W. Crane, " Wind speed prediction accuracy and expected errors of RANS equations in low relief inland terrain for wind resource assessment purposes." *Environmental Modelling & Software 26 (4), 429-433*, 2011.

[71] P. Fernando, W. Wu, H. Lu, and R. Conzemius, "Large-eddy simulation of atmospheric boundary layer flow through wind turbines and wind farms." *Journal of Wind Engineering and Industrial Aerodynamics 99, 154-168*, 2011.

[72] R. Stull, *An Introduction to Boundary Layer Meteorology.* Kluwer Accademic Publisher, 1988.

[73] H. Panofsky and J. Dutton, *Atmospheric Turbulence: Models and Methods for Engineering Applications.* John Wiley and Sons, pp.107-156, 1984.

[74] B. Blocken and C. Gualtieri, "Ten iterative steps for model development and evaluation applied to Computational Fluid Dynamics for Environmental Fluid Mechanics." *Environmental Modelling & Software 33 (2012), 1-22*, 2012.

[75] I. Castro and A. Robins, "The flow around a surface mounted cube in a uniform turbulent shear flow." *Journal of Fluid Mechanics 79(2), 307-335*, 1997.

[76] Y. Gao and W. Chow, "Numerical studies on airflow around a cube." *Journal of Wind Engineering and Industrial Aerodynamics 93(3), 115-135*, 2005.

[77] J. Franke, A. Hellsten, H. Schlunzen, and B. Carissimo, "The Best Practise Guideline for the CFD simulation of flows in the urban environment : an outcome of COST 732." in *Proceedings of The Fifth International Symposium on Computational Wind Engineering (CWE2010)*, Chapel Hill, North Carolina, USA, 2010.

[78] Y. Uematsu and N. Isyumov, "Wind pressures acting on low-rise buildings ." *Journal of Wind Engineering and Industrial Aerodynamics 82, 1-25*, 1999.

[79] G. Richardson, A. Roberston, R. Hoxey, and D. Surry, "Full-scale and model investigations of pressures on an industrial/agricultural building." *Journal of Wind Engineering and Industrial Aerodynamics 36, 1053-1062*, 1991.

[80] H. Okada and Y. Ha, "Comparison of wind tunnel and full scale pressure measurement tests on the Texas Tech building." *Journal of Wind Engineering and Industrial Aerodynamics 41-44, 1601-1612*, 1992.

[81] M. Levitan and K. Mehta, "Texas Tech field experiments for wind loads Part I: building and pressure measuring system." *Journal of Wind Engineering and Industrial Aerodynamics 41-44, 1565-1576*, 1992.

[82] ——, "Texas Tech field experiments for wind loads Part II: meteorological instrumentation and terrain parameters." *Journal of Wind Engineering and Industrial Aerodynamics 41-44, 1577-1588*, 1992.

[83] R. P. Selvam, "Computation of Pressures on Texas Tech Building." *Journal of Wind Engineering and Industrial Aerodynamics 41-44, 1619-1627*, 1992.

[84] ——, "Computation of flow around Texas Tech building using $k-\epsilon$ and Kato-Launder $k-\epsilon$ turbulence model." *Engineering Structures 18(11), 856-860*, 1996.

[85] A. Mochida, S. Murakami, M. Shoji, and Y. Ishida, "Numerical Simulation of Flowfield around Texas Tech Building by Large Eddy Simulation." *Journal of Wind Engineering and Industrial Aerodynamics 46 & 47, 455-460*, 1993.

[86] R. P. Selvam, "Computations of pressures on Texas Tech University building using large eddy simulation." *Journal of Wind Engineering and Industrial Aerodynamics 67 & 68(3), 647-657*, 1997.

[87] H. Jianming and C. C. S. Song, "A numerical study of wind flow around the TTU building and the roof corner vortex ." *Journal of Wind Engineering and Industrial Aerodynamics 67 & 68(3), 547-558*, 1997.

[88] B. Launder and D. Spadling, "The numerical computation of turbulent flows." *Computer Methods in Applied Mechanics and Engineering 3(2), 269-289*, 1974.

[89] ANSYSInc., "CFX Solver Theory Guide," 2014.

[90] R. Yoshie, A. Mochida, Y. Tominaga, H. Kataoka, K. Harimoto, T. Nozu, and T. Shirasawa, "Cooperative project for CFD prediction of pedestrian wind environment in Architectural Institute of Japan." *Journal of Wind Engineering and Industrial Aerodynamics 95, 1551-1578*, 2005.

[91] T. Fu, A. Aly, A. Chowdhury, and G. Bitsuamlak, "A proposed technique for determining aerodynamic pressures on residential homes." *Wind and Structures, Vol. 15, No. 1, 27-41*, 2012.

[92] J. Franke, C. Hirsch, A. Jensen, H. Krus, M. Schatzmann, P. Westbury, S. Miles, J. Wissie, and N. Wright, "Recommendation on the use CFD in wind engineering," https://www.kuleuven.be/bwf/projects/annex41/protected/data/Recommendations2004.

[93] D. Rehman, M. Naqvi, and I. Akhtar, "Proper orthogonal decomposition of pressure field behind bluff bodies." in *Proceedings of 10th International Bhurban Conference on Applied Sciences and Technology (IBCAST2013)*, Bhurban, Pakistan, 2013.

[94] L. Cochran and R. Derickson, "A physical modeler's view of Computational Wind Engineering." *Journal of Wind Engineering and Industrial Aerodynamics 99, 139-153*, 2011.

[95] C. Zang, B. Gong, and Z. Wang, "Experimental and theoretical study of wind loads and mechanical performance analysis of heliostats." *Solar Energy 105, 48-57*, 2014.

[96] C. Menna, D. Asprone, G. Caprino, V. Lopresto, and A. Prota, "Numerical simulation of impact tests on GFRP composite laminates." *International Journal of Impact Engineering 38, 677-685*, 2011.

[97] Y. Wang, J. Li, and D. Zhao, "Mechanical properties of fiber glass and kevlar woven fabric reinforced composites." *Composites Engineering 5(9), 1159-1175*, 1995.

[98] G. Belingardi, A. Beyene, and E. Koricho, "Geometrical optimization of bumper beam profile made of pultruded composite by numerical simulation." *Composite Structures 102, 217-225*, 2013.

[99] "AT & Standard Profiles 2014," availableathttp://www.alumil.com/files/1/Products/, 2014.

A

Log files for Structural simulation

```
FINISH  ! Make sure we are at BEGIN level
KEYW,PR_SET,1
KEYW,PR_STRUC,1
/GO
/PREP7
!****** Material Definition ********!
MPTEMP,1,0
MPDATA,EX,1,,73e9
MPDATA,PRXY,1,,0.35

MPDATA,EX,2,,26.66e9
MPDATA,EY,2,,21.07e9
MPDATA,EZ,2,,10.75e9
MPDATA,PRXY,2,,0.13
MPDATA,PRYZ,2,,0.34
MPDATA,PRXZ,2,,0.13
MPDATA,GXY,2,,5.17e9
MPDATA,GYZ,2,,5.05e9
MPDATA,GXZ,2,,5.04e9
!****** Keypoints for Geometry*****!
K, 1,0,0,0,
K, 2,0,2,0,
K, 3,2.5,2,0,
K, 4,2.5,0,0,
K, 5,0.5,0.7,0.4,
K,6 ,0.5,1.3,0.4,
K,7 ,1.1,1.3,0.4,
K,8 ,1.1,0.7,0.4,
!******** Lines from Keypoints *********!
LSTR,       1,       2  !L1
LSTR,       2,       3  !L2
LSTR,       3,       4  !L3
LSTR,       4,       1  !L4
LSTR,       5,       6  !L5
LSTR,       6,       7  !L6
LSTR,       7,       8  !L7
LSTR,       8,       5  !L8
LSTR,       2,       6  !L9
LSTR,       1,       5  !L10
LSTR,       7,       3  !L11
LSTR,       8,       4  !L12
!******* Area formation from Lines*******!
AL,1,5,9,10
AL,2,9,6,11
AL,7,12,3,11
AL,8,10,4,12
AL,6,5,8,7
KWPAVE,5
wpoff,0.05,0,0
wpro,,,90.000000
ASBW,5
KWPAVE,8
wpoff,,,-0.05
ASBW,7
!******** Defining Elements***********!
ET,1,SHELL181 ! Shell element for skin
KEYOPT,1,1,0
KEYOPT,1,3,0
KEYOPT,1,8,1
KEYOPT,1,9,0
ET,2,BEAM188  ! beam Element for Metallic supports
KEYOPT,2,1,0
KEYOPT,2,2,0
KEYOPT,2,3,0
KEYOPT,2,4,2
KEYOPT,2,6,0
KEYOPT,2,7,2
KEYOPT,2,9,3
KEYOPT,2,11,0
KEYOPT,2,12,0
KEYOPT,2,15,0
/PNUM,ELEM,0
aplot
!****** Sections Definition for beam and shell elements**
SECTYPE,   1, BEAM, HREC, beam, 4   ! First section is na
SECOFFSET, CENT
*set,W1,0.030 ! Width of cross beam section
*set,W2,0.030 ! Height of cross beam section
```

```
*set,t1,0.002 ! Thickness from first side
*set,t2,0.002 ! Thickness from second side
*set,t3,0.002 ! Thickness from third side
*set,t4,0.002 ! Thickness from 4th side
SECDATA,W1,W2,t1,t2,t3,t4,0,0,0,0,0,0 !W1,W2,t1,t2,t3,t4: For details of geometric variables, plea
sect,2,shell,,  ! Second section is defined for skin with shell elements
secdata, 0.003,1,0.0,3  !Aluminum skin for transition ring
secoffset,MID
seccontrol,,,, , , ,
!***** Assigning meshing attribites to all the areas of the skin*****!
AATT,       1, ,   1,       0,   2
!****Line Division for meshing**********!
FLST,5,8,4,ORDE,6
FITEM,5,1
FITEM,5,5
FITEM,5,7
FITEM,5,3
FITEM,5,15
FITEM,5,18
CM,_Y,LINE
LSEL, , , ,P51X
CM,_Y1,LINE
CMSEL,,_Y
LESIZE,_Y1, , ,30, , , , ,1
/PNUM,LINE,1
lplot
FLST,5,4,4,ORDE,4
FITEM,5,6
FITEM,5,8
FITEM,5,13
FITEM,5,-14
CM,_Y,LINE
LSEL, , , ,P51X
CM,_Y1,LINE
CMSEL,,_Y
!*
LESIZE,_Y1, , ,3, , , , ,1
FLST,5,2,4,ORDE,2
FITEM,5,19
FITEM,5,-20
CM,_Y,LINE
LSEL, , , ,P51X
CM,_Y1,LINE
CMSEL,,_Y
!*
LESIZE,_Y1, , ,24, , , , ,1
FLST,5,2,4,ORDE,2
FITEM,5,2
FITEM,5,4
CM,_Y,LINE
LSEL, , , ,P51X
CM,_Y1,LINE
CMSEL,,_Y
!*
LESIZE,_Y1, , ,30, , , , ,1
FLST,5,4,4,ORDE,2
FITEM,5,9
FITEM,5,-12
CM,_Y,LINE
LSEL, , , ,P51X
CM,_Y1,LINE
CMSEL,,_Y
!*
LESIZE,_Y1, , ,35, , , , ,1
FLST,2,3,4,ORDE,3
FITEM,2,8
FITEM,2,13
FITEM,2,19
LCCAT,P51X
FLST,2,3,4,ORDE,3
FITEM,2,6
FITEM,2,14
FITEM,2,20
LCCAT,P51X
MSHKEY,1
AMESH,1
AMESH,2
AMESH,3
```

```
AMESH,4
MSHKEY,0
CM,_Y,LINE
*SET,_Z1,LSINQR(0,13)
*IF,_z1,ne,0,then
LSEL,R,LCCA
*SET,_Z2,LSINQR(0,13)
LDELE,ALL
*SET,_Z3,_Z1-_Z2
*IF,_Z3,NE,0,THEN
CMSEL,S,_Y
CMDELE,_Y
*ENDIF
*ELSE
CMSEL,S,_Y
CMDELE,_Y
*ENDIF
MSHKEY,1
AMESH,6
AMESH,8
AMESH,5
MSHKEY,0
/PNUM,SECT,1
/REPLOT
AGEN,2,all, , , , ,10, ,0
ASEL,S,LOC,Z,0,5
ALLSEL,BELOW,AREA
aclear,all
ADELE,all
LDELE,      15, , ,1
LDELE,      18, , ,1
lplot
LATT,1, ,2, , , ,1
lmesh,all
ASEL,S,LOC,Z,0,15
ALLSEL,BELOW,AREA
AGEN,2,all, , , , ,-10, ,0
aplot
ASEL,S,LOC,Z,8,15
ALLSEL,BELOW,AREA
aclear,all
ADELE,all, , ,1
ALLSEL,ALL
!******** Pressure Load Application************!
SFA,1,1,PRES,-133.023
SFA,2,1,PRES,50.6066
SFA,3,1,PRES,-133.188
SFA,4,1,PRES,-93.1377
SFA,8,1,PRES,147.014
!******** Nodal Components to apply Displacement constrai
ASEL,R, , ,       6
ALLSEL,BELOW,AREA
WPCSYS,-1,0
CSYS,4
KWPAVE,      28
NSEL,U,LOC,X,0
NSEL,U,LOC,Y,0
KWPAVE,      27
NSEL,U,LOC,X,0
NSEL,U,LOC,Y,0
nplot
CM,udf1,NODE
allsel,all
ASEL,R, , ,       5
ALLSEL,BELOW,AREA
KWPAVE,     33
NSEL,U,LOC,X,0
NSEL,U,LOC,Y,0
KWPAVE,     30
NSEL,U,LOC,X,0
NSEL,U,LOC,Y,0
nplot
CM,udf2,NODE
allsel,all
!******* All Dof restriction on selected nodal components
CMSEL,S,UDF1
D,all, , , , , ,ALL, , , , ,
allsel,all
```

```
CMSEL,S,UDF2
D,all, , , , , ,ALL, , , , ,
allsel,all
/replot
CPINTF,ALL,0.0001, ! Coupling all conincident nodes
!***** Solution**********!
FINISH
/SOL
ANTYPE,0
NLGEOM,1
NSUBST,10,500,5
OUTRES,ERASE
OUTRES,ALL,ALL
TIME,1
SOLVE
```